Investigation of NiO/Potato Peels Nanocomposite Prepared through Hydrothermal Method

By

AYESHA ANJUM

CIIT/FA21-RPH-025/LHR

MS Thesis

In

Physics

COMSATS University Islamabad

Lahore Campus-Pakistan

Spring, 2023

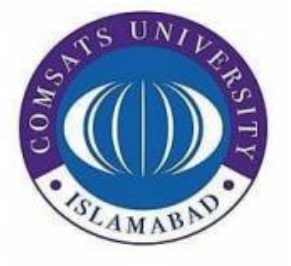

COMSATS University Islamabad

Investigation of NiO/Potato Peels Nanocomposite Prepared through Hydrothermal Method

A Thesis Presented to

COMSATS University Islamabad, Lahore Campus

In partial fulfillment
of the requirement for the degree of

MS (Physics)

By

Ayesha Anjum

CIIT/FA21 -RPH-025/LHR

Spring, 2023

Investigation of NiO /Potato Peels Nanocomposite Prepared through Hydrothermal Method

A post-Graduate Thesis submitted to the Department of Physics as partial fulfillment of the requirement for the Degree of MS (Physics) award.

Name	Registration Number
AYESHA ANJUM	CIIT/FA21-RPH-025/LHR

Supervisor

Dr. Mukhtar Ahmad
Associate Professor
Department of Physics
COMSATS University Islamabad,
Lahore Campus

Final Approval

This thesis is titled.

Investigation of NiO /Potato Peels Nanocomposite Prepared through Hydrothermal Method

By

Ayesha Anjum

CIIT/FA21-RPH-025/LHR

Has been approved.

For the COMSATS University Islamabad, Lahore Campus

External Examiner: _____

Dr. Ghulam Murtaza

Associate Professor, center for advance study in Physics, GC University, Lahore

Supervisor: _____

Dr. Mukhtar Ahmad

Associate Professor, Department of Physics, CUI, Lahore

HOD: _____

Prof. Dr. Muhammad Asif

HOD (Department of Physics) CUI, Lahore

Declaration

I Ayesha Anjum, student of MS(Physics) registration number CIIT/FA21-RPH-025/LHR hereby declare that I have completed this research work and presented it in the form of a thesis within the research schedule. I also declare that in this thesis there is no copied material except those taken as reference. If any violation of HEC rules occurred in research work, I will be personally held responsible and liable to be punished under plagiarism rules fixed by HEC.

Date: ————— Signature of the student

_____

Ayesha Anjum

CIIT/FA21-RPH-025/LHR

Certificate

It is to be certified that Ms. Ayesha Anjum student of MS physics having registration number CIIT/FA21-RPH-025/LHR has completed this research work under my supervision. She is a regular student of the Department of Physics COMSATS Institute of Information Technology Lahore, and her research work fulfills the requirement for the award of an MS degree.

Date: ————————

Supervisor:

_____

Dr. Mukhtar Ahmad
Associate Professor,
Department of Physics,
COMSATS University
Islamabad Lahore campus

Head of Department:

_____

Prof. Dr. Muhammad Asif
Department of Physics COMSATS University
Islamabad Lahore campus

DEDICATION

I dedicate my work to ALLAH Almighty who gives me the strength to move on and to my father, my mother, and my husband. I could not have done this without you. Thank you for all your support along the way.

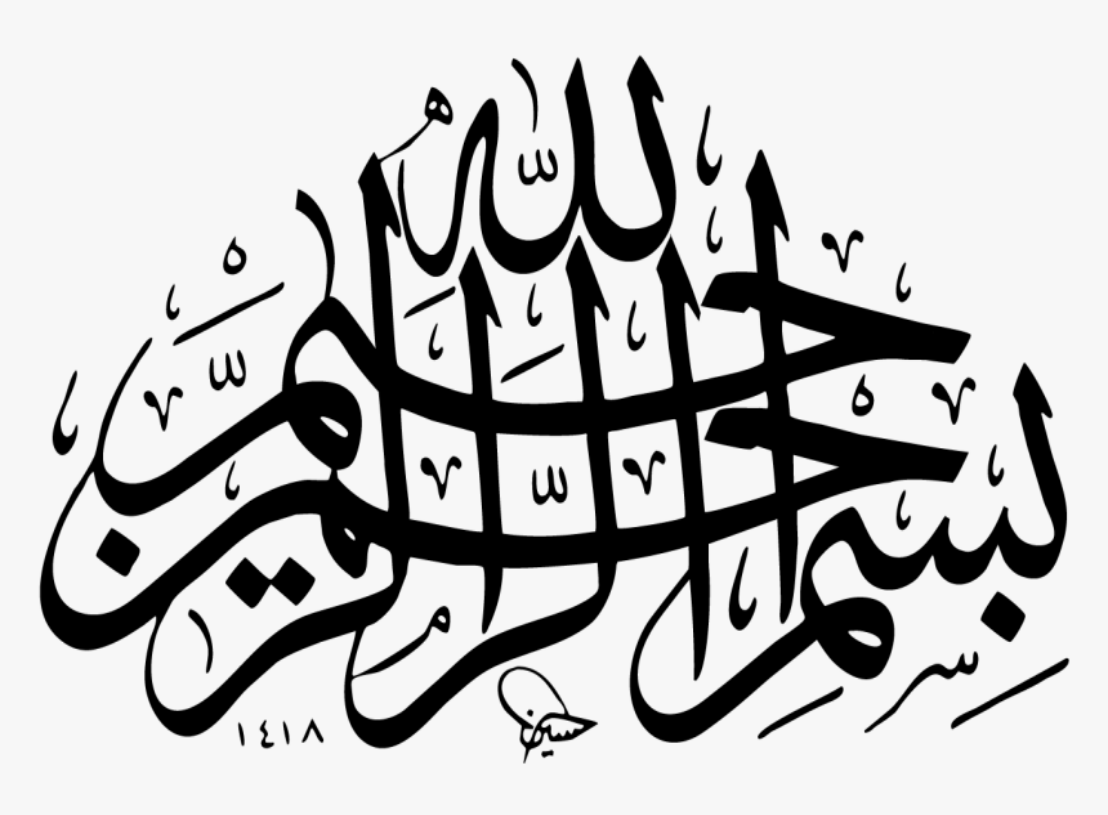

IN THE NAME OF ALLAH,

THE MOST BENEFICIAL,

THE MOST MERCIFUL.

ACKNOWLEDGMENTS

I am very thankful to **ALLAH** who created us and sprinkles His blessings upon us. **ALLAH** blesses us and sends His Beloved Last Prophet **HAZRAT MUHAMMAD (PBUH)** for the guidance of human beings. We all Muslims love **HAZRAT MUHAMMAD (PBUH)** who teaches us the principles of Islam. He **(PBUH)** is our noble and ideal teacher.

I sincerely thank my supervisor, **Dr. Mukhtar Ahmad**, for leading me through research. Their positive attitude towards research and zest for research work has prompted me for the timely completion of the work. Thank you for continually inspiring me to do my best, you help me strive for goals. I found guidance discipline and love everything in one person. Instead of leading me by holding my hands, you asked me to walk ahead while you caringly observed from behind.

I am thankful to my father whose striving efforts, adorable behavior, and financial and moral support in each step of my life make me strong and drive me through my thick and thin circumstances.

Above all, I thank to Almighty Allah for providing me with valuable opportunities in my life with Shuker and Sabar, who helped and encouraged me.

Ayesha Anjum

CIIT/FA21-RPH-025/LHR

ABSTRACT

Investigation of NiO /Potato Peels Nanocomposite Prepared through Hydrothermal Method

One of the most important problems in the world today is the fluoride pollution of the surrounding waters due to activities and anthropogenic activities. Due to their high catalytic activity and large surface area, ferrite nanoparticles have gained interest in wastewater treatment. Synthesis of NiO/Potato Peels Nanocomposites using a hydrothermal process to remove fluoride from drinking water is exported in the present study. Various tests such as X-ray diffraction (XRD), scanning electron microscopy (SEM), and Fourier transmission infrared spectroscopy (FTIR) are used to identify the structure and morphology of the composite. The XRD results identified a single-phase structure with lattice parameters ranging from 8.38Å to 8.33Å. Agglomerated and heterogeneous-sized nanoparticles are seen in SEM micrographs. FTIR depicts the ranges of NiO within the repetitiveness range of 400–4000 cm^{-1}. These incorporation bands, situated at 665 cm^{-1} and 543 cm^{-1}, pertain to the extended shaking modes of the tetrahedral ore-oxygen bond and the octahedral ore-oxygen bond, individually.

TABLE OF CONTENTS

LIST OF FIGURES

List of Tables

CHAPTER 1

INTRODUCTION

1 Nanotechnology

Nanotechnology has become one of the most important technologies across all study fields. Norio Taniguchi, a scientist from Japan, is credited for developing nanotechnology at the beginning [1].Over time, the use of this discipline increased and was eventually widespread in several sectors, including biology, electronics, and material sciences [2,3]. Nanoparticles can connect bulk materials with atomic or molecular structures, which is of great scientific interest [4]. Nanotechnology is the study and use of structures with sizes ranging from one nanometer (nm) to one hundred nanometers. Structures, electronics, and systems all have unique properties and functionalities due to the arrangement of their atoms on a scale of 1 to 100 at the nanoscale [5].

1.1 Nanotechnology Applications

Now that you know the basics of nanotechnology, let's see how it can be used to clean wastewater. Nanotechnology can be used to clean wastewater by removing various impurities in it. Nanoparticles are special for their off-the-shelf use because the nano process removes all impurities [6].

TiO2, ZnO, ceramic membranes, nanowire membranes, polymer membranes, carbon nanotubes, submicron nano-powders, metal (oxides), magnetic nanoparticles, nanostructured boron-doped diamond, and other nanoparticles, etc. The high specific surface area, rapid disintegration, strong reactivity, and strong adsorption of nanoparticles make water visible and make it cost-effective to use nanotechnology for wastewater treatment.

An important part of the rapid development of nanotechnology is the production of nanoparticles and nanoproducts with specific and size-dependent physicochemical properties, unlike bulk products. [7]. Many successful applications in biomedicine, cosmetics, healthcare, renewable energy, and environmental remediation take advantage of the unique properties of nanoparticles. [8-10].

Nanoparticles have excellent optical, electrical, magnetic, and catalytic abilities due to their high volume-to-volume ratios compared to bulk materials.

[11,12]. Silver and gold nanoparticles are metals with different colors due to the phenomenon of plasmon resonance (SPR). Surface plasmon resonance bands are visible in

the infrared spectrum due to group oscillations of free electrons in metal nanoparticles that resonate with the interaction of light waves. [13].

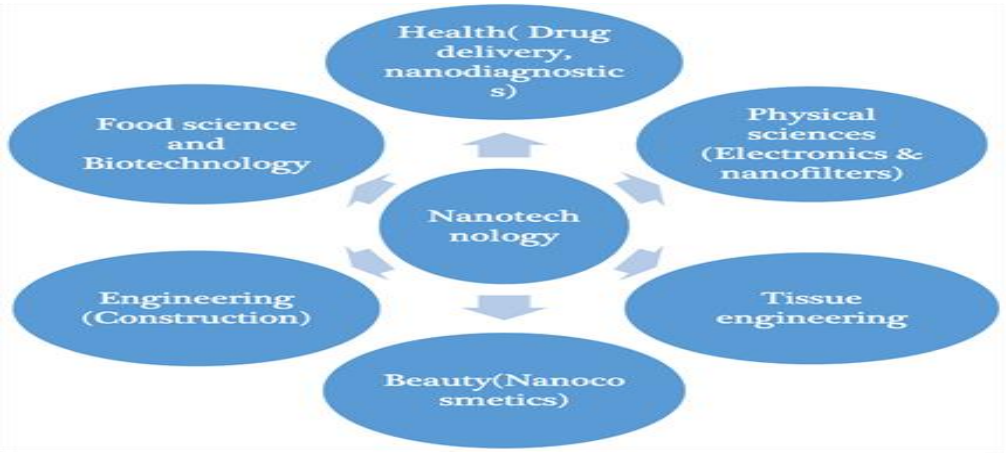

Figure 1.1: Applications of Nanotechnology

1.1.1 Nanoparticles and Applications of Nanoparticles

Over the past ten years, there has been a considerable increase in the fabrication of nanoparticles with programmable morphologies and exceptional capabilities, opening a large new field of study. One of the primary objectives in chemistry has been the production of nanoparticles (NPs) with precise control over their diameter, structure, and crystallinity. Only a few possible applications for these NPs include biosensors, bio-medical devices, low-cost electrodes, and catalysts for bacterial biotoxin clearance [14-16].

Alternatively, we can define nanoparticles as a collection of physically or chemically linked atoms with a structural radius smaller than 100 nm. Compared to the world of commonly encountered things that are represented by Newton's laws of motion, a nanoparticle is much smaller but larger than an atom or a molecule [17-18].

In addition, nanoparticle-based solar cells and catalysts offer promising opportunities for renewable energy generation and chemical transformations.

1.2 History of Magnetism

Thales of Miletus, a Greek philosopher, first mentioned the Lodestone in his writings around 600 BCE, marking the beginning of magnetism. The contemporary name "magnet"

is derived from an early lodestone discovered in the Greek province of Magnesia, Anatolia [19-22].

The Book of the Devil Valley Master, written in 400 BCE, has the oldest Chinese mention of the word "Lodestone." The second-century BC author Lushi Chunqiu said that lodestone "attracts" or "makes" iron come to it. Chinese navigators began utilizing Lodestone compasses in the 12th century.

William Gilbert, an English scientist, was the first to study magnetism using rational means in 1600. Gilbert experimented extensively with his model of the Earth, known as the Terrella.

1.3 Basic of Magnetism

1.1.1 Magnetization

The magnetic dipole moment induced per unit volume of the substance is known as magnetization (M). Ampere/meter is its SI unit [23]. The emu/cm3 is the cgs unit of magnetism. Mathematically,

$$M = \frac{m}{V} \frac{emu}{cm^3} \text{ in cgs} \quad (1.1)$$

M = magnetization

M = magnetic moment

V = volume of the material

1.1.2 Magnetic Induction

The outcome of applying a magnetic field (H) to a material is known as the material's magnetic induction (B). The connection between B and H is one of the elements of the content. The following equation (in cgs units) connects B with H. The magnetic induction unit is known as the "Gauss"

$$\mathbf{B = H + 4\pi} \quad (1.2)$$

1.1.3 Magnetic Flux Density

The magnetic induction, B, is equal to the flux density inside the medium. Therefore, by similarity with H=/A in space, B=/A within a material.

The formula for the relationship between B, H, and M in SI units is

$$B=(H+M) \quad (1.3).$$

where o is the open space's permeability [25]. Weber/m2, or tesla (T), is the SI unit for B; 1 gauss is equal to 10^{-4} tesla.

1.1.4 Magnetic Susceptibility

Magnetic Susceptibility is defined as the relationship between the strength of the applied magnetic field and the intensity of magnetization [26].

Mathematically

$$X_m = \frac{M}{H} \qquad \frac{emu}{cm^3 Oe} \tag{1.4}$$

A material's susceptibility to a magnetic field can be used to gauge how responsive it is.

1.1.5 Magnetic Permeability

The definition of magnetic permeability of a material is "the ratio of magnetic induction to the magnetic field intensity" [27]. Mathematically,

$$\mu = \frac{B}{H} \qquad \frac{gauss}{Oe} \tag{1.5}$$

μ describes a material's magnetic field permeability. A material has a high permeability when a significant amount of flux density is concentrated inside of it.

1.3.6 Relation between Magnetic Permeability and Susceptibility

The link between permeability and susceptibility can be determined using the formula B=H+4M.

$$B = H + 4\pi M \tag{1.6}$$

$$\frac{B}{H} = 1 + 4\pi\frac{M}{H} \tag{1.7}$$

$$\mu = 1 + 4\pi X \tag{1.8}$$

1.1.6 Hysteresis Loop

A hysteresis loop, sometimes referred to as a hysteresis curve, is a four-quadrant graph that depicts the interaction between the magnetizing force H and the induced magnetic flux density B [28-30]. It is frequently called the B-H loop. We may infer a variety of magnetic properties of a material via hysteresis loops. Retentivity, residual magnetism (or residual flux), coercive force, permeability, and reluctance are a few examples.

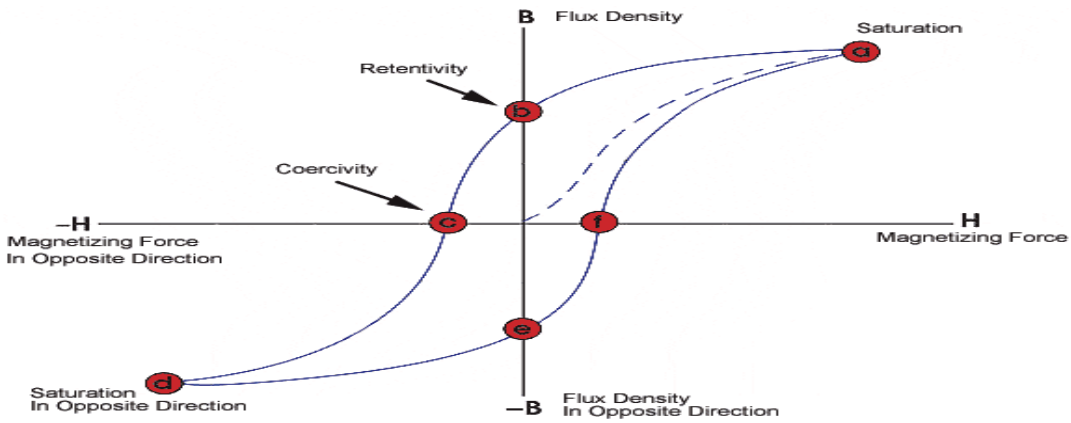

Figure 1.2: Hysteresis Loop

Hysteresis loops are an important property of ferromagnetic materials that are widely used in many applications such as magnetic materials and magnetic materials. Understanding the behavior of hysteresis loops is essential for the design and development of such devices [30].

1.2 Classification of Magnetic Materials

A magnetic material is magnetic, i.e., can attract or repel other magnetic materials. These materials can be divided into five groups according to their magnetic properties:

- Diamagnetic materials
- Paramagnetic materials
- Ferromagnetic materials
- Antiferromagnetic materials
- Ferrimagnetic materials

1.2.1 Diamagnetic materials

Diamagnetic materials are repelled by magnetic fields because they produce magnetic fields to form in the opposite direction of the one being applied, creating an attractive force. A few examples include cobalt, nickel, and iron.

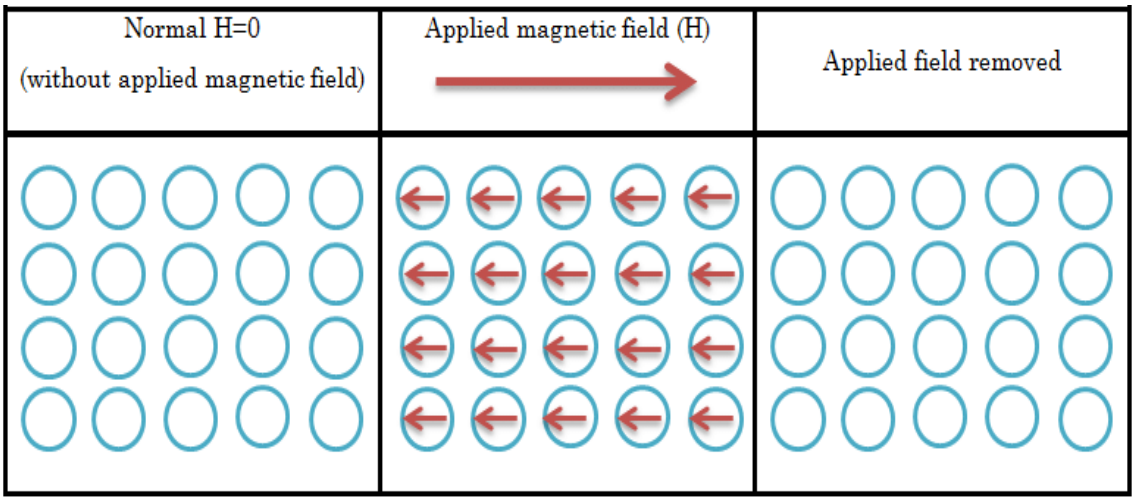

Figure 10.3: Diamagnetic materials

1.2.2 Properties of Diamagnetic Materials

• Since electrons combine, the magnetic moment of each atom is zero, that is, diamagnetic materials do not have atomic dipoles.

• Antimagnetic materials do not stick to magnets.

• In an inhomogeneous environment, materials tend to move from strong to weak external magnetic fields, as the magnetic field repels them weakly.

• The magnetization (I) is proportional to the magnetic field and is a very small negative value.

• Magnetic susceptibility is very small and insignificant.

• The permeability rate is just below [31-32].

1.2.3 Paramagnetic Materials

Some electrons in paramagnetic materials are unpaired and the net magnetic moment of all electrons in an atom is not equal to zero. So, in this case, atomic dipoles exist. When an external magnet is used, the direction of the external magnetic field causes the atomic dipoles to align.

This results in a weak magnetic field in the direction of the magnetization field of the paramagnetic material [33].

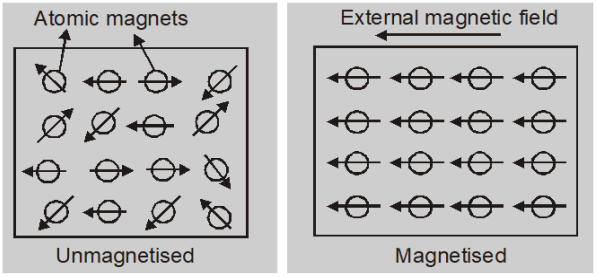

Figure 1.04: Paramagnetic material

1.2.4 Properties of Paramagnetic Materials

Paramagnetic materials

• Atoms have a net nonzero atomic dipole moment whereas atoms of paramagnetic materials have a permanent dipole moment due to unpaired spin.

• The magnetic field attracts the material very little.

• Paramagnetic materials move from a weak point to a strong point if the external magnetic field is not homogeneous. Because the field is strong near the pole, the paramagnetic rods merge with the field.

• Paramagnetic fluid rises between the poles of a magnet in a U-shaped tube.

• Magnetization is positively and negatively related to magnets.

• Good to moderate magnetic susceptibility is present.

1.2.5 Ferromagnetic Materials

The permanent atomic magnetic moments in some materials have great alignment ability even in the absence of an external field [34]. These materials are called ferromagnetic materials. Cobalt, iron, nickel, gadolinium, dysprosium, permalloy, avarice, write, and magnetite are some examples of ferromagnetic materials.

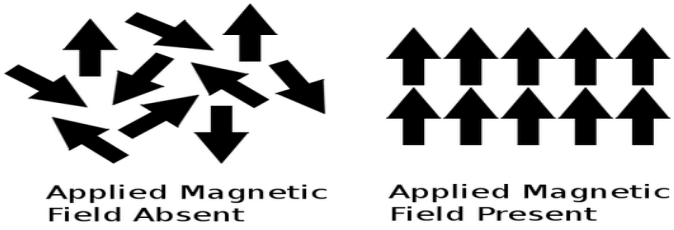

Figure 1.5: Ferromagnetic material

1.2.6 Properties of Ferromagnetic Materials

Ferromagnetic material

• When exposed to a magnet, the magnetic field of this material quickly transforms into a magnetic field.

• Some compounds are magnetically stable even without a magnetic field.

• Ferromagnetic materials change from ferromagnetic to paramagnetic when heated at high temperatures.

• Ferromagnetic materials with magnetic permeability greater than 1.

• There is no ferromagnetic mechanism in liquids and gases.

• Natural materials have positive magnetic flux density (B), magnetic susceptibility (m), magnetic susceptibility strength (M), and relative magnetic permeability (r).

1.2.7 Anti-ferromagnetic Material

Antiferromagnetic (a type of magnetic repulsion) occurs when the magnetic moments of nearby atoms or ions align together, creating a zero magnetic moment. This behavior is caused by exchange interaction between nearby atoms or ions, which tend to combine to reduce the energy of the system.

Below a specific temperature called the Neel temperature, most antiferromagnetic materials exhibit magnetic order. Beyond that, the material becomes paramagnetic and loses its antiferromagnetic. [35].

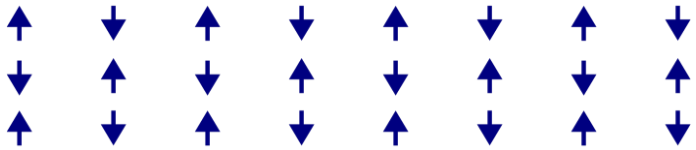

Figure 1.06: Anti-ferromagnetic material

1.2.8 Properties of Anti-ferromagnetic Material

• Antiferromagnetic materials hold the same promise as spintronic materials, which use spintronic electrons instead of charges to act as information and storage.

• Antiferromagnetic materials are less sensitive to external magnetic fields because they have no inherent magnetic moments, making them ideal for stable and reliable materials.

• Antiferromagnetic materials can be used in magnetic field sensors, especially those using a negative exchange. When an antiferromagnetic material is bonded to a ferromagnetic

material, the ferromagnetic hysteresis loop changes, causing the change to change. This variant can be used for the detection of weak magnetic fields in a variety of applications, including diagnostic and security systems.

• Antiferromagnetic materials used in MRAM; a magneto resistive random-access memory [36].

1.2.9 Ferrimagnetic Material

According to the definition of ferrimagnetic materials, random net magnetization results from the opposition of magnetic dipoles of atoms in different subsets, as in antiferromagnetic materials.

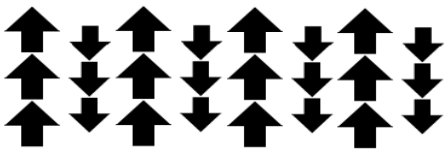

Figure 1. 7: Ferrimagnetic Material

1.3.10 Properties of Ferrimagnetic Materials

- Ferrimagnetic material has high resistivity and anisotropy properties. Anisotropy is caused by external influences. When an applied field is aligned with a magnetic dipole, the magnetic dipole can rotate at a frequency modulated by the applied field, called the Larmor or precession frequency.
- This gives the net magnetic dipole moment. For example, in a circularly polarized microwave pulse in the same direction as the precession associated with the magnetic dipole moment, the effect is very small when the pulse is polarized in the opposite direction.
- When the contact is stable, the microwave signal will pass through the device. This routing ability is used by devices that use microwave energy, such as splitters, circulators, and gyrators. Ferrimagnetic materials are also used to make optical devices and circulators. Ancient [37-38].

.

1.3 Purification of Water

1.3.1 Water Pollutants

We have long held the view that water is an abundant, naturally occurring resource that is a gift from nature and essential for maintaining both life and the environment. The chemical makeup of the water, whether at the surface or below, is one of the most important factors in determining whether it is safe for use in residential, commercial, or agricultural settings. Freshwater can be obtained from both surface water and groundwater. Despite making up only 0.6% of the world's total water resources, groundwater is the primary and most widely used source of drinking water. It provides 50% of the water needed for agricultural use and 80% of the total demand for drinking water. But in our period, groundwater pollution is increasing due to urbanization and industrialization. [39-41].

1.3.2 Methods of water purification

The various techniques used to purify water can be categorized in a variety of ways. As a result, attempts to develop efficient methods for treating wastewater contaminated with heavy metals have greatly expanded [42]. These methods include chemical precipitation, ion exchange, membrane filtration, coagulation/flocculation, electrochemical treatment, and adsorption. The most frequently researched and applied in the industry is adsorption [43]. For the removal of fluoride from the aqueous medium, a variety of adsorbent materials have been researched and reported, including activated alumina, zeolites, brick powder, activated carbon modified with KMnO4, bauxite, Kanuma mud, and many others. Additionally, a variety of plant-based biosorbents have been researched recently and claimed to have varied degrees of effectiveness for removing fluoride from water, including dried orange juice residue, tamarind (Tamarindus indica) fruit shell carbon, and Moringa.

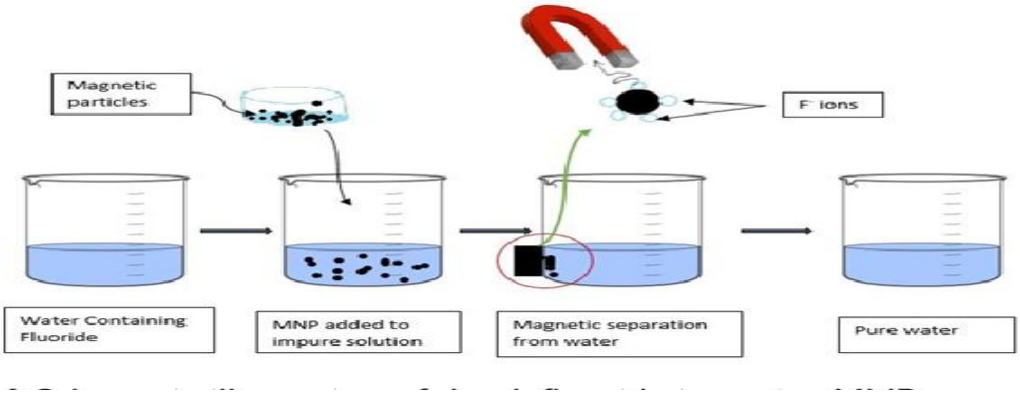

Figure 1.0 8: Adsorption Method

1.3.3 Purification of Water using Ferrite

Ferrite treatment is one of the most promising methods for enhancing impurity removal from water and wastewater. The findings of theoretical and experimental studies of ferrite water and wastewater are presented in this publication.

Treatment is provided by the company Invite. Three plants (industrial locations) with capacities ranging from 1 to 8 m3/h and varied surface water sources underwent pilot investigations. Currently, two ferrite-based wastewater treatment facilities for electroplating are in operation. The process was studied experimentally, and the reaction chamber for the ferrite-treated water was modeled. According to calculations, this development has a smaller cost burden than is typical in the field. [44-47].

1.3.4 Purification of Water using Ferrite/biowaste composites

Potato, also known as Azedarach India, is a big, evergreen tree that is regarded as a "Saratoga Navarino" (remedy for all diseases). In the past, a variety of adsorbent substances have been used to find a defluorination agent that is both effective and affordable. Some adsorbents include potato peel, groundnut shell, rice husk, neem leaves, coffee husk, and orange peel powder. Potato peels are used as bio-sorbents for the adsorption of fluoride since they are naturally abundant and affordable. In this study, we used potato peel powder, as an active adsorbent to remove fluoride from water. Potato Peel has a porous structure and so can absorb more Fluoride ions from water [48-50].

CHAPTER 2

LITERATURE REVIEW

Literature Review

Due to its prospective applications, the study of NiO/Potato Peels Nanocomposite Prepared via the Hydrothermal Method is relevant in many disciplines. This chapter's literature review tries to present a thorough examination of the current research on this subject. This study aims to pinpoint knowledge gaps and aid in future developments in this field by looking at the synthesis, characterization, and applications of the nanocomposite.

Materials called nanocomposites blend nanoparticles with a matrix substance to produce materials with characteristics and capabilities. Due to their numerous uses in industries including electronics, energy storage, catalysis, and environmental clean-up, they have attracted a lot of interest. The numerous forms of nanocomposites, their synthesis techniques, and their relevance in various sectors will all be covered in this section. The creation of nanocomposites is frequently accomplished by the process of hydrothermal synthesis. The ideas behind the hydrothermal process will be discussed in this part along with how they apply to the creation of NiO/Potato Peels Nanocomposite. The benefits of employing aqueous solutions at high temperatures and pressures, as well as the hydrothermal method's ability to regulate particle size, morphology, and crystallinity, will be explored.

NiO nanoparticles have special qualities that make them useful for a variety of uses. The features and attributes of NiO nanoparticles, including their magnetic, optical, and catalytic capabilities, will be covered in detail in this section. Additionally, it will examine the various synthesis techniques used to produce NiO nanoparticles, with a focus on the hydrothermal technique. We will review prior research on hydrothermal methods for the manufacture and characterization of NiO nanoparticles. An easily available biomass waste with potential uses in a variety of sectors is potato peels. The chemical makeup, quantity, and other characteristics of potato peels will all be covered in this section. Additionally, it will go through possible uses for potato peels in a variety of industries, including the use of food industry waste, biodegradable materials, and renewable energy.

This section will examine earlier works that looked into the hydrothermal method's use in the synthesis and characterization of NiO/Potato Peels Nanocomposite. Each study's main

contributions, techniques, and key conclusions will be outlined. This review looks at the available literature to find any gaps or restrictions that require additional study.

A summary of the major themes covered in the chapter on the literature review will be given in this section. The importance of the current study in filling in the known gaps or resolving the literature's inadequacies will be emphasized. A summary of the remaining chapters of the thesis will also be given, detailing the research methods, experimental strategy, and anticipated results.

Two examples of energy storage technologies with a lot of potential in a variety of applications are supercapacitors and lithium-ion batteries. Here, NiO-porous carbon composites were synthesized via a straightforward, green technique employing discarded banana peels. The NiO-porous carbon composite's surface shape and chemical makeup were

(Al Kiey, S. A., & Hasanin, M. S. (2021)) EDX and a scanning electron microscope (SEM) were used to conduct the investigation. The produced samples were also described using surface area measurements, thermal gravimetric analysis (TGA), x-ray powder diffraction (XRD), and Fourier transform infrared (FTIR) spectroscopy. Using cyclic voltammetry (CV), galvanostatic charge-discharge, and electrochemical impedance (EIS), the electrochemical behavior of the materials was examined to see if they were suitable for use as supercapacitor electrodes. The PC-NiO (3) composite has a high specific capacitance of 811 F/g at a current density of 1 A/g. The specific capacitance of PC-NiO (3) is 5.3 times higher at 1.0 A/g than that of PC material. The figures above show that the high specific capacitance of the NiO-porous carbon nanocomposite makes it one of the most promising electrode materials for supercapacitors.[51]

(Suvaitha, S. P., Sridhar et al 2022) Large-scale production and disposal of biowaste is a major issue that exists everywhere in the world. Chemically converting biowaste resources into products with functional carbon is one of the environmentally favorable methods. In this study, the hydrothermal carbonization process was used to create biochar from the readily accessible potato peel waste, and KOH was used to activate the carbon. Copper phthalocyanine (Cu-Pc), which is a highly nitrogen-enriched substance, was coupled with the activated carbon substance (Pot) to generate a composite material (Cu-Pc/Pot).

Cyclic voltammetry (CV), galvanostatic charge-discharge (GCD), and electrochemical impedance spectroscopy (EIS) were used to examine the electrochemical behaviors of the synthesized materials. At 0.1 Ag-1 current in a 1 M H2SO4 aqueous electrolyte, the composite material exhibits an excellent capacitance value of 237 F/g. Up to 1000 cycles at 1Ag-1, the material also demonstrates long cycling stability. These results dispelled any uncertainty regarding the suitability of Cu-Pc/Pot composite material as an electrode material for electrochemical supercapacitor energy storage applications. [52]

(Suvaitha, S. P., Sridhar et al 2022) To regulate the particle size, a bio-waste eggshell membrane was used as a template in this study's synthesis of a NiO/ZnO nanocomposite. Soaking is the first stage, and then the calcination procedure is used. The following methods were used to characterize the synthesized NiO/ZnO nanocomposite: Powdered X-ray diffraction analysis (PXRD), Ultra-Violet Visible spectroscopy (UV-Visible), Fourier transformed infrared spectroscopy, Raman spectroscopy, Dynamic Light Scattering analysis (Zeta potential & particle size), Field Emission SEM- The NiO/ZnO nanocomposite can be found in both face-cantered cubic (NiO) and hexagonal wurtzite (ZnO) forms, according to PXRD experiments.

NiO and ZnO crystallite sizes were 14.12 nm and 14.70 nm, respectively, in size. The wavelengths at 302 nm and 372 nm in the UV-Visible spectrum were indicative of the presence of ZnO and NiO, respectively. The stretching vibration of (Ni-O) NiO2 octahedral in cubic NiO and the stretching vibration of ZnO are responsible for the peaks at 449 cm1 and 550 cm1, respectively. A Raman vibrational mode helps the NiO/ZnO nanocomposite to develop. The NiO/ZnO nanocomposite's 42.7 mV zeta potential value was determined by measurements, which is a positive indicator of stability. The polydispersity index was 0.5940, and the estimated particle size distribution was 205.8 nm. The NiO/ZnO nanocomposite looked to be aggregated with small rods in the SEM pictures.

The presence of nickel, oxygen, and zinc was all confirmed by the EDX spectra. The particle size of the NiO/ZnO nanocomposite was less than 50 nm, according to TEM images. The synthesized NiO/ZnO nanocomposite's antibacterial and antifungal activity was evaluated using the agar-well diffusion method. The NiO/ZnO nanocomposite's minimum inhibitory concentration (MIC) against bacterial pathogens was studied. The

results demonstrated that even at the minimum concentration (9.37 g/mL), the synthesized NiO/ZnO nanocomposite hindered cell proliferation. So, it is implied that a variety of ailments could be treated with the NiO/ZnO nanocomposite's antifungal and antibacterial properties. [53]

(Ullah, H., Mushtaq et al 2021) Effect of vegetable waste extract on microstructure, morphology, and photocatalytic efficiency of ZnO–CuO nanocomposites. *Inorganic and Nano-Metal Chemistry*, *51*(7), 963-975. We investigated the effects of waste extracts from three different vegetables (potatoes, peas, and cauliflowers) on the optical band gap (Eg), crystal structure, morphology, and photocatalytic effectiveness of ZnO-CuO. According to XRD and SEM results, the vegetable waste extract modified the crystallites' size and shape. The extract from vegetable waste also displayed significant fluctuation, much to how the broad Eg of n-type ZnO reduced when combined with p-type CuO.

The generated ZnO-CuO nanocomposites were used as photocatalysts for the degradation of an organic dye under visible light. The organic dye served as a model environmental contaminant in this experiment. It was revealed that under ZnO-CuO photocatalysts synthesized utilizing waste extracts from cauliflower, peas, and potatoes, respectively, 95.6%, 93%, and 91.3% of the dye degraded in 120 minutes. [54]

Eggshells are often regarded as trash since they are useless as food but encourage microbial development. Large amounts of eggshell trash are produced by the baking, food processing, and hatching industries.

The results showed that hydrothermal reaction times and biomolecule concentrations had an impact on product dimensions, shape, and synthetic HA crystal morphology. Pomelo peelings were used to extract HA, and this HA had good aspect ratios and physical forms that were similar to the crystalline HA formations found in actual human bone. Na, Mg, and Sr are some of the significant trace elements found in HA made from eggshell powders. [55]

(Ullah, H., Mushtaq et al 2019) It has been claimed that nickel oxide (NiO) nanostructures can be produced sustainably and cheaply. The waste from three distinct vegetables—cauliflower, potatoes, and peas—was extracted to produce the organic capping and/or

reducing agents. According to scanning electron microscopy, the extracts of potato peels produced nanorods of NiO whereas the extracts of cauliflower and pea peels produced nano-whiskers. All of the samples' nanocrystalline cubic phase of NiO was shown by X-ray diffraction investigations. However, the size of the crystallites varied depending on the vegetable waste extract employed. The identification of various vibrations, notably Ni-O stretching vibrations, using Fourier transform infrared analysis is helpful. Analyses of diffuse reflectance spectra helped establish bandgap energies. The effectiveness of the obtained NiO nanostructures as photocatalysts for the degradation of Methylene blue was evaluated.

All three samples had significant photocatalytic activity. The investigation in this paper unequivocally shows the very effective photocatalytic activities of the synthesized NiO nanostructures, which may be employed as reliable agents for wastewater treatment to eliminate harmful colors. [56]

(Narender, S. S., Varma et al 2022) Nanoparticles (NPs) are particles having a size between 1 and 100 nm, measured in any dimension. The physical, chemical, and biological characteristics of nickel oxide nanoparticles (NNPs), one type of nanoparticle, make them significant. Significant research has been conducted on the synthesis of NNPs during the past 20 years. Their uses include catalysis, energy storage, and antifungal and antibacterial action. This review gives a quick rundown of several of the procedures for creating NNPs, as well as their characteristics and uses. Physical synthesis, chemical synthesis, and green synthesis using plants and microorganisms, particularly fungi, are the several types of synthesis techniques. The types of precursors employed in their synthesis, as well as their morphology, particle size, and uses, are the subjects of particular attention. [57]

(Vishnukumar, P., Saravanakumar et al 2018) The solvothermal approach was used to create nickel oxide/nickel vanadate ($NiO/Ni_3V_2O_8$) nanocomposites with regulated size and form. The precursor solution of nickel chloride and ammonium metavanadate was dissolved in a solvent with sodium hydroxide acting as a reducing and stabilizing agent. By adjusting the solvothermal processing period as 10 hours, 14 hours, and 18 hours at 160°C, three distinct products were produced. $NiO/Ni_3V_2O_8$formation is supported by X-ray diffraction (XRD), Fourier-transform infrared (FTIR), Raman, and photo luminescence

(PL) experiments. Studies using a field emission scanning electron microscope (FESEM) give precise details on the configuration of $NiO/Ni_3V_2O_8$nanorods. To comprehend the pseudocapacitive characteristics of the produced compounds, electrochemical investigations were conducted. Due to the regular arrangement and consistent size distribution of the nanorods, the estimated specific capacitance for product PVK1 has a better value of 653 Fg^{-1} at current density 1 Ag^{-1}. [58]

(Pirathiba, S., & Dayananda, B. S. 2021) Due to its aid with factors like increased firmness, stimulating activity, and loading amount, nanoparticle biogenesis, particularly gold and silver nanoparticles, has been applied increasingly. These ultrafine particles are created by decreasing and capping potato skin waste extract with more environmentally friendly chemicals. The study uses leftover potato skin that isn't worth anything to make nanoparticles quickly at room temperature. The creation of green nanoparticles and their representation were made possible by the results of the UV-visible spectrophotometer, scanning electron microscopy (SEM), energy dispersive X-ray analysis (EDAX), X-ray diffraction analysis (XRD), and Fourier transform infrared spectroscopy (FTIR). Results of a UV-visible spectral analysis on the production of silver nanoparticles indicate that the absorbance value peaks between 420 and 440 nm.

The absorbance value for gold nanoparticles was similar, falling between 530 and 560 nm. According to SEM findings, the produced gold and silver nanoparticles were spherical in shape and ranged in size from 10 to 20 nm for gold nanoparticles and 20 to 40 nm for silver nanoparticles. Silver and gold nanoparticles exhibit greater peaks in the EDAX spectrum, indicating that the particles were very pure when they were produced. The atomic plane phases (11 1) and (1 2) were prevalent in nanoparticles, according to SEM results that agreed with XRD analyses. The produced silver and gold nanoparticles were discovered to have amide and amine groups (i.e., proteins) cap them from the FTIR spectrum. The potato's amylose and amylopectin aldehydes function as a reducer. One of the work's intriguing aspects is that it used vegetable peel waste, as opposed to most mature works, which were restricted to the use of plant extract. [59]

(Liang, S., & McDonald, A. G. 2014) The growing demand for renewable fuels has generated interest in utilising alternative waste materials, such as potato peel waste (PPW),

which contains fermentable carbohydrates. About 60% of the PPW fermentation residue (PPW-FR) produced by a mixed microbial consortium employed to ferment PPW was unreacted. The PPW and PPW-FR were analyzed using a combination of Fourier transform infrared (FTIR), nuclear magnetic resonance (NMR), gas chromatography-mass spectrometry (GC-MS), and thermogravimetric analysis (TGA), to measure modifications post fermentation.

By fermenting starch and concentrating lignin, suberin, and lipids, the fermentation of PPW resulted in PPW-FR. The breakdown peaks for PPW (423 °C) and PPW-FR (457 °C), respectively, were different, according to TGA analysis. After fermentation, pyrolysis-GC/MS analysis of the PPW revealed an increase in phenolic and long-chain fatty acid components and a concurrent decline in chemicals derived from carbohydrates. Based on their characteristics, the PPW and PPW-FR have both demonstrated the ability to be thermochemically processed into crude biofuel. [60]

CHAPTER 3

RESEARCH METHODOLOGY & CHARACTERIZATION TECHNIQUES

3. Research Methodology and Characterization Techniques

This section consists of two parts. The first chapter will present the hydrothermal process for the production of Nickle oxide (NiO) with potato peel composites. The second section will focus on the various methods used to analyze the structure, morphology, and magnetic properties of Nickle oxide (NiO) with potato peel.

Section 1

3.1 Synthesis Techniques

There are many techniques that can be used to create patterns. The list below contains some popular methods,

- Hydrothermal technique
- Co Precipitation technique
- Micro-emulsion technique
- Microwave technique
- Sol-gel technique
- Ball milling technique

The hydrothermal technique is used in this research work to produce the sample.

3.2 Hydrothermal Synthesis

The word "hydrothermal" is derived from the words "hydraulic" and "thermal", denoting water and heat, respectively [61]. The idea behind the hydrothermal method is that using high temperatures, insoluble materials can be put into a furnace at high temperatures and then converted into soluble solutions. The growth process takes place in an autoclave, which is a pressure vessel made of metal containing a solvent and water [62]. By controlling the temperature and reaction time, we can easily precipitate the powder from the solution. Any heterogeneous chemical process can be used with this method.

Temperatures below 300°C are sufficient for hydrothermal synthesis. This technique was first used in the mid-19th century when submicron materials were processed to produce nanometer-sized objects. This method was applied from the 1840s to the early 1990s because there were no methods that could characterize nanomaterials. This technique was used in the 1980s after the revolution in nanomaterials [63]. Hydrothermal/solvothermal synthesis is widely used to prepare nanomaterials with crystallinity, morphology and

crystals due to its good properties such as small additive, reaction in aquatic environment, low energy consumption and environmental friendliness. The stage of the twenty-first century [64].

Ferrites, on the other hand, have been produced using hydrothermal processes at temperatures between 150 and 200 °C without the use of heat treatment processes or calcination processes [65]. The significant improvement in the reagent is one of the advantages of hydrothermal synthesis.

3.2.1 Features of Hydrothermal Method

The hydrothermal process has the following features [66].

- Ability to process materials at melting points with high vapor pressure.
- Selection of materials that are unstable at high temperatures.\
- Materials that cannot be produced by conventional methods can be obtained by hydrothermal methods.
- Suitable for large and fine crystals

3.2.2 Factors Affecting Crystal Growth in the Hydrothermal Method

Controlling the following variable parameters could result in the end products having the preferred particle sizes and morphologies [67].

3.2.3 Chemical Factors

- ❖ Nature of solvent
- ❖ Nature of the seed
- ❖ Nature of the nutrient

3..2.3 Physical Factors

- ❖ Temperature of crystal growth
- ❖ Pressure
- ❖ Hydrodynamics of the system

3.2.4 Kinetic Factors

- ❖ Diffusion of species
- ❖ Kinetics of dissolution
- ❖ Duration of the crystal growth

3.3 Sample Preparation

3.3.1 Required Material for Sample Preparation

1. Nickel Chloride
2. Sodium hydroxide
3. Potato Peels

Table 3.1: Material Required for Sample Preparation

Sr. no.	**Chemical name**	**Molecular formula**	**Molar mass**	**Supplier**
1	**Nickel Chloride**	$NiCl.6H_2O$	237.69 g/mol	Sigma-Aldrich
2	**Sodium hydroxide**	NaOH	39.997 g/mol	Sigma-Aldrich

3.3.2 Required Steps for Sample Preparation

The synthesis of a sample of Nickel Oxide with potato peels, using the hydrothermal process includes the following steps.

- Measurement of chemicals
- Preparation of solutions
- Mixing and stirring of solutions
- Addition of NaOH
- Washing
- Autoclave
- Drying
- Grinding

3.3.3 Measurement of Chemicals for Sample Preparation

After stoichiometry, we derived the required chemical concentrations for the various samples, as indicated in Table 3.2

Table 3.2: Measurement of Chemicals

Sample no.	Sample name	Chemical	Quantity
Sample-1	NiO	$NiCl.6H_2O$	2.37 g/mol
		NaOH	0.79 g
Sample-2	NiO/Potato Pees 10ml	$NiCl.6H_2O$	2.37 g
		NaOH	0.79 g
		Neem leaves extract	10 ml
Sample-3	NiO/Potato Pees 20ml	$NiCl.6H_2O$	2.37 g
		NaOH	0.79 g
		Neem leaves extract	20 ml
Sample-4	NiO/Potato Pees 30ml	$NiCl.6H_2O$	2.37 g
		NaOH	0.79 g
		Neem leaves extract	30 ml

3.3.4 Weighting of the Materials

Rinse the spatula with deionized (DI) water before using it to prepare the sample solution. Then, using the electronic equipment carefully, measure the solution with a spatula and some aluminum foil.

Figure 0.1: Electronic Balance

3.3.5 Preparation of the Solution

Prepare each precursor solution using 25 mL of deionized (DI) water, then prepare a homogeneous solution from each stock weight to prepare the cap chloride, manganese chloride, ferric chloride, and sodium chloride solution.

3.3.6 Mixing and Stirring of Precursors

Stirring using a magnetic stirrer. Use deionized water to clean the magnetic palette before placing it in the beaker with precursor and deionized water.

Figure 0.2: Magnetic Stirrer / Hot Plate

Mix the prepared solutions of copper chloride, manganese chloride and ferric chloride in a 500 ml beaker. After mixing for 30 minutes, we finally got a homogeneous solution.

3.3.7 Addition of NaOH

The NaOH solution was added dropwise to the solution with constant stirring. The NaOH addition was completed in 90 minutes. When we add NaOH, a precipitate starts to form.

3.3.8 Washing

In the process of adding NaOH, copper chloride, manganese chloride, ferric chloride, and sodium hydroxide react to produce copper manganese chloride, and sodium chloride. Sodium chloride is an impurity and dissolves in water, so it must be washed away. For cleaning, fill the beaker containing the solution with deionized water and stir for 15 minutes. After 5 hours the precipitate was at the bottom of the beaker and the water was removed from the top. This process was done several times to remove all of the sodium chloride.

3.3.9 Autoclave

After washing, the solution is poured into polytetrafluoroethylene in the autoclave and then the autoclave is heated at 200°C for 6 hours. When materials are heated, the bond between them breaks. The water evaporates and they spread over each other [68]. Leave the autoclave outside of the oven until it reaches room temperature at the end of the autoclave period.

Figure 0.3: Autoclave

3.3.10 Drying

If the samples are completely dry, they can be ground into a fine powder. Dry samples were obtained by placing the beaker containing the samples in an oven at 90°C for 5-6 hours to dry.

3.3.11 Grinding

Grind the samples using a mortar and pestle. The sample is crushed to obtain better homogeneity and smaller particle size.

Figure 0.4: Pestle and Motor

3.3.12 Sintering

After pulverization, the sample was transferred to a ceramic cup and placed in an oven for sintering at 600°C for 5 hours. Single-phase core ferrites are produced by evaporation of all impurities. After the value is sinered, it is finely crushed into powder with pestle and mortar and then pressed into powder pellets.

Figure 0.5: Electrical Furnace

3.3.13 Packing of the material

For future behavior and future use, use a spatula to place the samples on the labels.

Figure 0.6: Bullet Box

3.4 Procedure

- The first sample S-1 was prepared according to the steps listed below. Initially, two beakers 200ml beakers containing 50ml each of DI water were used.
- After that, weighted amounts of sodium hydroxide and nickel chloride were combined with water in separate beakers using magnetic stirring.
- In a 500 ml beaker, the above- mentioned solutions (nickel chloride) were then homogenized. NaOH solution was poured to this beaker while it was being stirred constantly.
- After that, this solution was rinsed to eliminate the sodium hydroxide. After washing, the mixture was vacuum-sealed in an autoclave and heated for five hours at 200°C.
- The prepared sample was placed in a beaker once the autoclave had cooled to room temperature, and it was then dried for 5–6 hours at 90°C in the oven.
- After removing all the moisture, the sample was ground up and put in a bullet box for further examination. S2, S3 and S4 were all prepared using the same method, but with varying amounts of potato peels added to the earlier precursors.

Section 2

3.5 Characterization Techniques

The material is characterized using the following techniques:

- X-ray diffractometer (XRD)
- Scanning Electron Microscope (SEM)
- Fourier-Transform Infrared spectroscopy (FTIR)

3.5.1 X-Ray Diffraction

X-ray diffraction is one of the most important techniques for analyzing the properties of samples [69]. The crystal structure of materials can be studied using the non-destructive XRD technique [70,71]. Each material produces a diffraction pattern, which is a type of crystallographic fingerprint used to describe the properties of the sample.

Here are the components of a typical XRD setup.

- Photodiode
- Laser
- Sample surface

3.5.2 Working Principle of X-Ray Diffraction

Good reflection follows Bragg's law, which is the basis of X-ray diffraction. For X-ray wavelengths, the crystal structure acts as a three-dimensional (3D) diffraction grating. The reflected pattern of monochrome X-rays is formed by the crystal structure. According to Bragg's law, the wavelength of the incident radiation affects the diffraction angle and the distance from the plane [72,73].

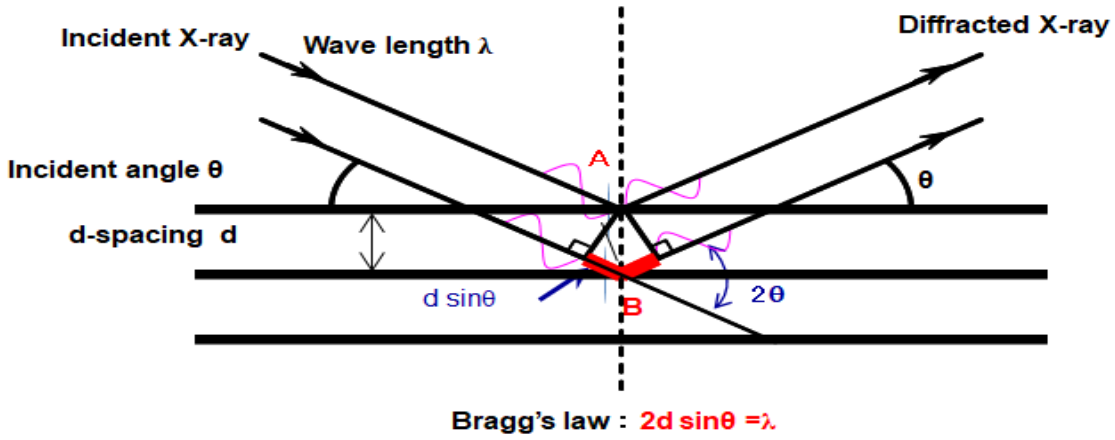

Figure 0.7: Bragg's law, X-ray Diffraction from atoms in a Crystalline Sample

In X-ray diffraction, parallel beams of X-rays are reflected on the sample, and diffraction is done by the crystalline phase in the sample. According to the Bragg equation, the wavelength of the X-ray beam is between 0.5 and 2Ao.

$$n\lambda = 2d\sin\theta \tag{3.1}$$

The distance between atomic planes in the crystal phase is represented by the letter "d".

The diffraction angle 2 and sample orientation are used to calculate the intensity of the diffraction X-rays [74]. The size, direction, and properties of the sample phase (eg, visible and nasal) are determined by the diffraction pattern and can be used to describe the crystalline phase of the sample. In addition, atomic configuration, film thickness, and defects can be determined using XRD [75]. This equation is used to determine the lattice parameter "a".

$$d = \frac{a}{\sqrt{h^2+k^2+l^2}} \tag{3.2}$$

The Debye-Scherer formulacan also be used to determine the size of crystal diffraction peaks.

$$D = \frac{0.9\lambda}{\beta COS\theta} \tag{3.3}$$

where "D" denotes crystal size, "**λ**" X-ray wavelength, and angular width [76]

3.5.3 X-Ray Diffraction Methods

The techniques used to examine the various properties of crystals are as follows:

- Single crystal rotation method
- Powder method
- Laue method

In the first two methods, the wavelength is constant while the angle is variable, in the Laue method the wavelength is fixed. angle as constant and variable [77,78].

3.5.4 Powder Method

In this method, a very fine powder sample is exposed to a monochrome X-ray beam.According to Bragg's law, this ray is reflected by the sample in all directions. Rotate the model in various directions using a device called a protractor [79]. Some crystals are oriented in the (110) plane, while others are oriented in the [80] plane. This allows the light to be reflected from different angles and captured in the detector.

3.5.5 Application of XRD

- Material identification
- Quality control in pharmaceuticals
- Geological analysis
- Material characterization in materials science

- Forensic analysis

3.6 Scanning Electron Microscopy (SEM)

For analyzing grain morphology at extremely high resolution, scanning electron microscopy is a fantastic technique. SEMs offer extremely high resolution at the Angstrom level. SEMs employ cathode rays produced by cathode ray tubes. Electrons can be utilized to detect minute changes in a sample's surface since they move so quickly and have very little inertia [81-82]. The block diagram of a scanning electron microscope is shown in the diagram below.When cutting the sample with a microtome, it typically comprises electrical wires blasted from a stun gun and operates between 5 to thousands of volts. One of the most crucial is a vacuum. A diffusion pump must deliver 106 Torr of pressure to the tungsten filament. A vacuum is produced by the vacuum cleaner. Ion pumps may be utilised to lower pollution, depending on the application [83-84].

A goniometric connection in the sample chamber allows the sample to travel in three directions. Electricity is reflected by magnetic lenses. The electrical and electronic parts can be seen in the CRO camera as secondary radiation is emitted when the cathode beam destroys the sample [85-86]. It makes it easier for outer electrons to form and for electrons to scatter. Other electrons diffuse close to the edge, whereas backscattered electrons diffuse from below the surface.With the proper CRO and testing tools, stronger radiation may be released [87-88]. Two voltages are generated when the cathode ray strikes the semiconductor sample. In the present electrical structure, there are electron hole pairs. When light sources like solar cells or P-n junctions are nearby, it enters the light depletion zone and generates a current that automatically enters the models [89-90]. The following are the parts of a scanning electron microscope:

- Electron Source
- Magnetic Lens
- Scanning Coil
- Sample Chamber
- SEM Detector

The objective is used by SEM to analyse the material.A multitude of signals are created when the beam strikes the sample's surface, including secondary radiation that creates images, specialised X-rays from the research object, and blazing electrical vapours that release light and heat.

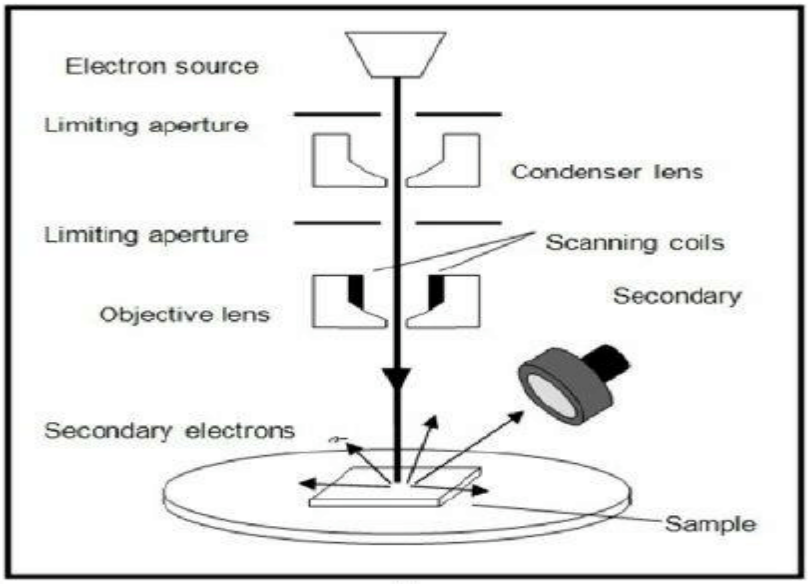

Figure 0.8: Scanning Electron Microscopy (SEM)

3.6.1 Modes of SEM

Three fundamental operating modes are possible for SEM.

3.6.2 Secondary Electron Detection Mode

Secondary electrons (less than 50eV) are electrons produced when primary electrons interact with the sample. In this mode, SEM produces good images.

3.6.3 Backscattered Electron Detection Mode

Elastic and inelastic scattering of the primary electron beam causes the generation of backscattered electrons.This type provides detailed information about crystal orientation, boundaries and composition [91].

3.6.4 X-Ray Detection Mode

Semiconductor diodes (PIN diodes) detect X-rays when electric light interacts with the sample. This mode provides detailed information about the base composition and the point-to-point distribution of the sample [92].

3.7 Fourier-Transform Infrared Spectroscopy

Raman spectroscopy can be performed by illuminating the sample with unidirectional laser light, which interacts directly with the sample molecules to produce light scattering. Raman spectra are produced by scattering light at a different wavelength than incoming light. Inelastic contact of unidirectional incident light with sample molecules produces Raman spectra. When it comes into contact with the sample molecules, the monochromatic light is scattered in all directions. Rayleigh scattering occurs when the frequency of the scattered radiation is related to the frequency of the incident radiation.

Raman scattering occurs when only a small portion of the scattered light has a different wavelength than the incident electron. Stokes lines are formed when the frequency of the incident radiation is greater than that of the radiation. Anti-Stokes lines can be detected when the frequency of the incident radiation is lower than that of the radiation. Radiation incident at right angles is the most common angle for radiation measurement [93]. The following components make up a typical Fourier transform infrared (FTIR) spectrometer:

- Radiation source
- Michelson interferometeRadiation detector

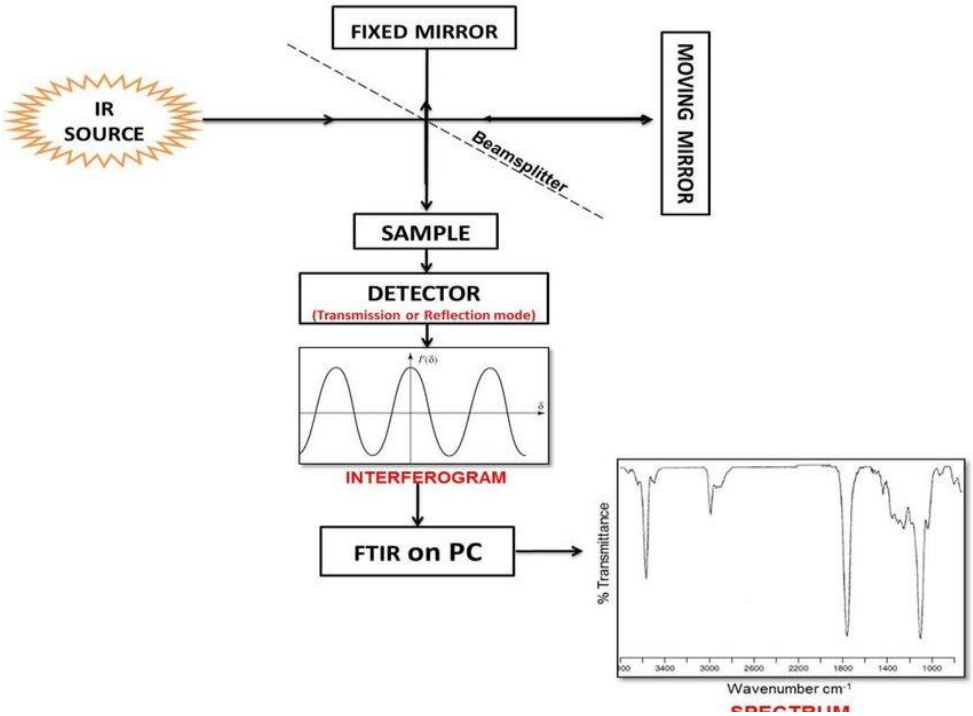

Figure 0.9: Schematic diagram of FTIR

CHAPTER 4

RESULTS AND DISCUSSION

4. Results and Discussion

4.1 X-ray Diffraction Analysis

Crystal structures of synthesized materials were determined by X-ray diffraction. The NiO with potato peels composite were predicted using diffraction peaks in the XRD. At a 2θ angle, the diffracted intensities were seen from 20° to 80°.

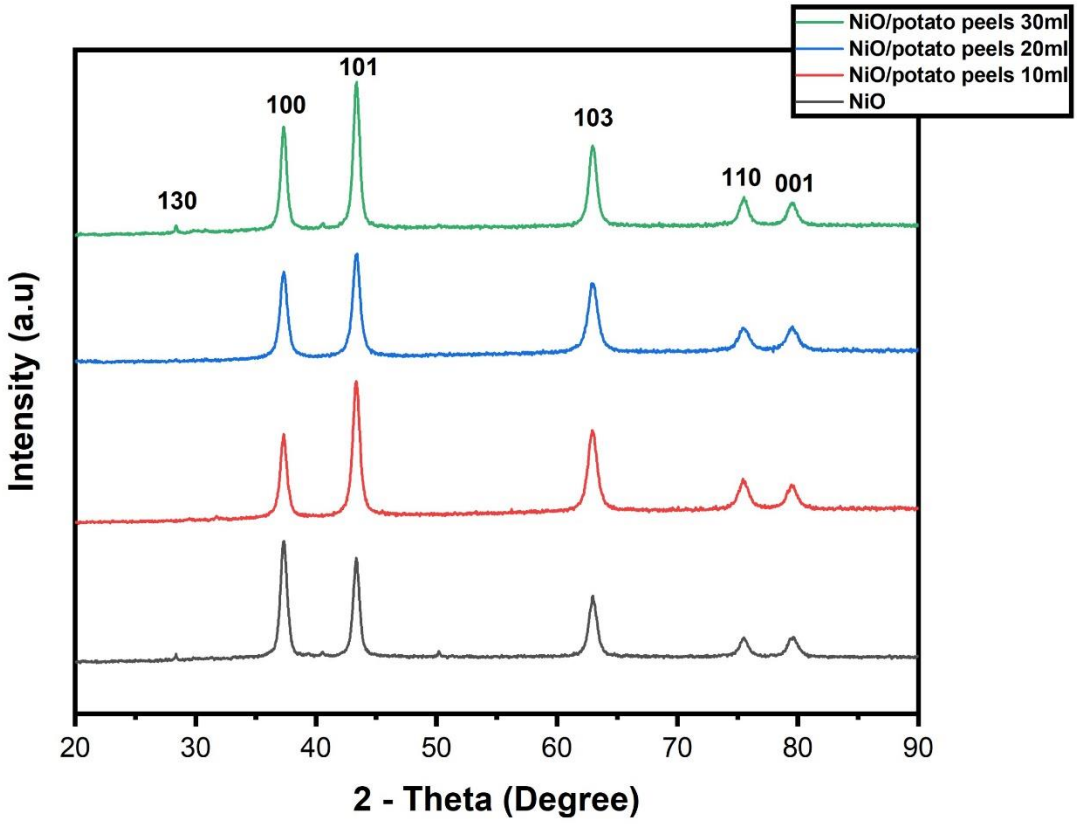

Figure 0: XRD results for all samples

The crystallinity of the NiO nanoparticles (NPs) has been shown by the discovered reflections in Figures 2. The Bragg reflections are indexed as h k l values: (130), (100), (101), (103), (110) and (001). The diffraction peaks of all the samples showed the characteristic of a phase- pure Ni-Zn ferrite spinel structure with the highest intensity peak obtained from (101) plane, which is comparable to the pure Nickel oxide XRD data. Because of the face-centered cubic (FCC) crystalline structure of NiO, all of these diffraction peaks may be precisely indexed to it.

their characteristic peaks' relative intensity, which is in line with the spectrum's standard value (JCPDS, No. 04-0835), is similar. The XRD pattern demonstrates that the samples are single-phase and that only the distinctive diffraction peaks of the FCC phase NiO were found. The diffraction peaks of the uncalcined and calcined nickel oxide nano powders closely matched the impurity peak, confirming the high purity of the NiO NPs made using the described method. For Nickel oxide, Nickel oxide /10ml potato peels, Nickel oxide /20ml potato peels, and Nickel oxide /30ml potato peels the lattice parameter is evaluated and determined to be 8.36Å ,8.38Å ,8.37Å and 8.33Å accordingly.

4.1.1 Lattice Constant (a)

Using the following equation, lattice constant (a) was calculated [94].

$$d = \frac{a}{\sqrt{h^2 + k^2 + l^2}} \qquad (4.1)$$

where (d) is the inter-planar spacing and (hkl) are miller indices. A drop in the lattice constant (a) from 8.36Å ,8.38Å ,8.37Å and 8.33Å is obtained as shown in table (4.1). The neem leaves' insertion to the NiO is what causes this decrease.

4.1.2 Crystallite Size (D)

By taking into account the Scherrer formula's greatest intensity diffraction peak (1 0 1), the crystallite size of these nanoparticles was determined.

$$D = \frac{0.9\lambda}{\beta\cos\theta} \qquad (4.2)$$

Table 4.1 shows that crystalline size is decreased with increasing the quantity of neem leaves extract.

4.1.3 Unit Cell Volume (V)

Employing the following relationship, the lattice parameter was utilized to evaluate the volume of the unit cell:

$$V = a^3 \qquad (4.3)$$

Unit cell volume is drop by adding neem leaves extract (table 4.1)

4.1.4 X-ray Density (D_X)

Using the equation below, the X-ray density of the produced samples was determined [93].

$$D_x = \frac{8M}{N_A a^3} \quad (4.4)$$

X-ray density increased from 5.77, 5.92, 6.11 and 6.26

4.1.5 Lattice Strain (ε%)

We use the following formula for calculating Lattice Strain:

$$\varepsilon = \frac{\beta}{4\tan\theta} \quad (4.5)$$

"β" belongs to the "full width half maxima" while "θ" denotes the Bragg's angle

4.1.6 Dislocation Density (δ)

Crystallite size was utilized to evaluate dislocation density (δ), and the formula is expressed as [95]:

$$\delta = \frac{15\varepsilon}{aD} \quad (4.6)$$

Where "ε" indicates lattice strain, "D" indicates crystallite size, and "a" represents lattice constant. Increasing the amount of neem leaves also enhances its value (Table: 4.1).

Table 4.1: Variation of structural parameters

Samples	**a (Å)**	**V (Å)**	**D_x (g/cm^3)**	**D (nm)**	**δ (Lines/m^2)**	**ϵ (%)**
S1	8.36	584.22	5.77	16.5	0.0249	0.249
S2	8.38	588.48	5.92	16.1	0.0225	0.258
S3	8.37	586.37	6.11	15.9	0.0372	0.384
S4	8.33	578.00	6.26	15.3	0.0315	0.368

4.2 Fourier Transforms Infrared Spectroscopy (FTIR)

Infrared spectroscopy is handled to decide the appropriate working groups present in the fabrics. Inside spinal ferrite fabrics, atoms are delivered across various sites famous as octahedral and tetrahedral sites. A Fourier alter color of blood spectroscopy (FTIR) test was administered to create NiO, and Figure 4.2 depicts the FTIR ranges of NiO within the repetitiveness range of 400–4000 cm-1. These incorporation bands, situated at 665cm-1 and 543 cm-1, pertain the extended shaking modes of the tetrahedral ore-oxygen bond and the octahedral ore-oxygen bond, individually. Uncalcined NiO powders' measured infrared

(IR) spectra highlight a number of significant characteristics. The existence of hydroxyl groups is first suggested by a wide band at 3126 cm1, which also shows the stretching vibrations of OH bonds. This band's width suggests that molecules have formed internal and external hydrogen bonds. Water molecules that are chemisorbed or physiosorbed on the surface of the particles are also indicated by a peak at 1636 cm1. The existence of carbon-hydrogen groups is shown by the band at 1245 cm1, which is ascribed to the angular distortion of C-H bonds.

The C-O ether bond vibrations of the glucose ring in starch can be attributed to two different peaks at 1087 cm^{-1}. Due to comparable characteristic absorption peaks, these data imply the existence of organic chemicals in the sample in addition to the new inorganic substance (Ni-O). This result is consistent with earlier research in the literature. Finally, the emergence of absorption bands at 485 cm1 provides evidence for the production of NiO nanoparticles by confirming the existence of stretching vibrations linked to the Ni-O bonds.

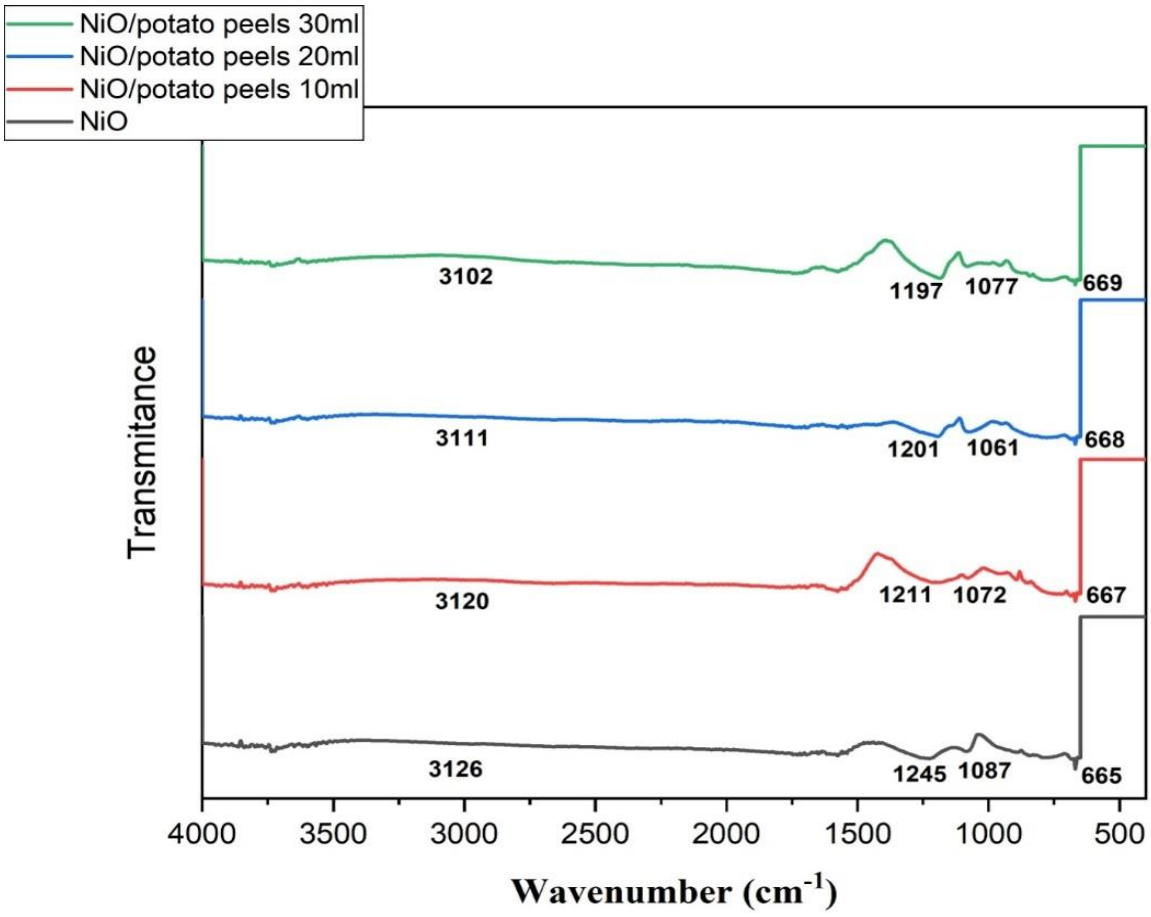

Figure 0: FTIR Results for all samples

4.3 Scanning Electron Microscopy

The morphologies of the formed materials were determined utilizing flipping through energized matter microscopy (SEM). SEM images of NiO (Figure 4.8) and NiO accompanying Vegetable Peels (Figure 4.9) tell that the resulting samples contain clusters of nanoparticles. The SEM micrographs apparently show non-uniform shapes and a sort of piece sizes. The SEM images determine a more apparent view of the piece accumulation. Neem leaves be a part of seed inhibitors, lowering the formation of ferrite nanoparticles when increased the ferrite. The wealth is used unevenly superficial. Carelessly scattered Potato Peels pieces of various sizes maybe observed alongside the Coat with metallic material Group of chemical elements atoms. The microstructure resides of a single type of piece, signifying the deficiency of any supplementary subordinate chapters. By employing foul line interrupt method, the average grain proportion for NiO and NiO/Vegetable Peels was persistent to be 500 and 229 nm, individually. As an alone seed consists of diversified crystallites, it has existed noticed that the seed size in each sample, established the Scherrer rule, is more the crystallite size.

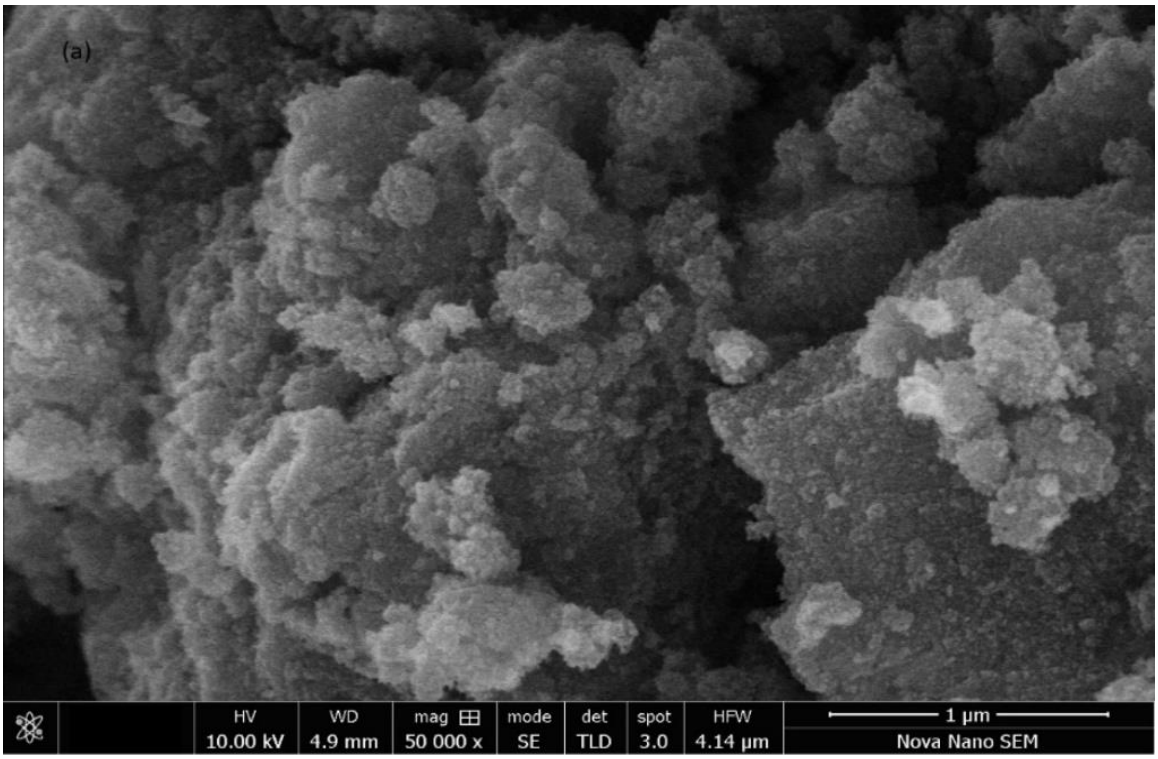

Figure 4.3: SEM Image of Nickel Oxide NiO

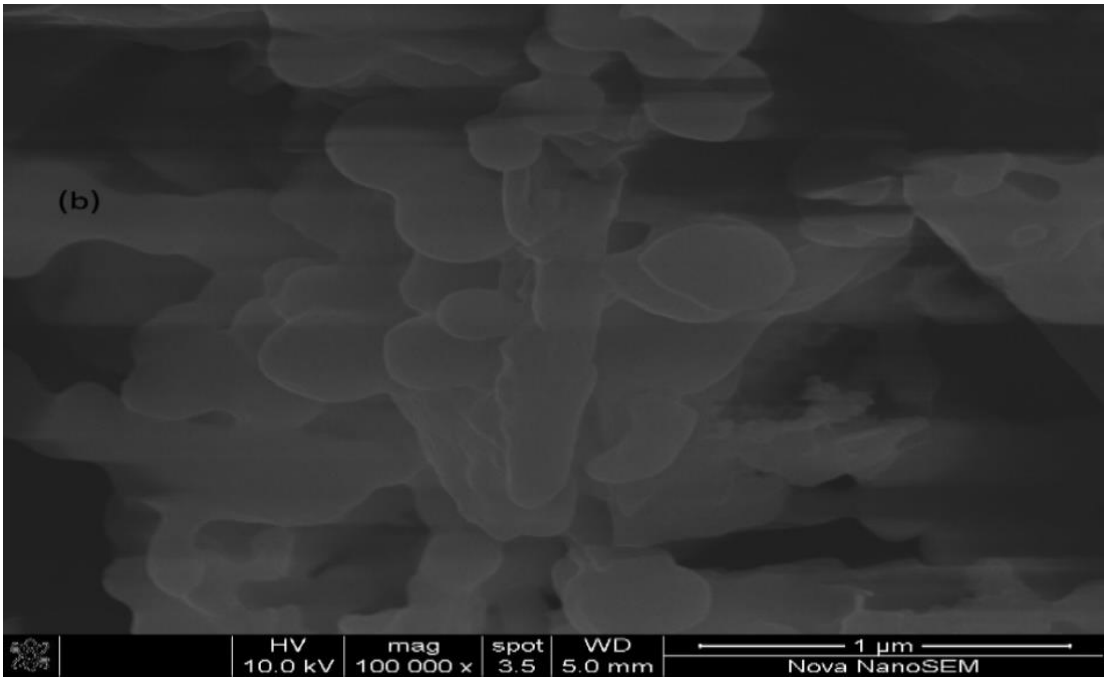

Figure 4.4: SEM Image of Nikel Oxide NiO / Potato Peels (10ml)

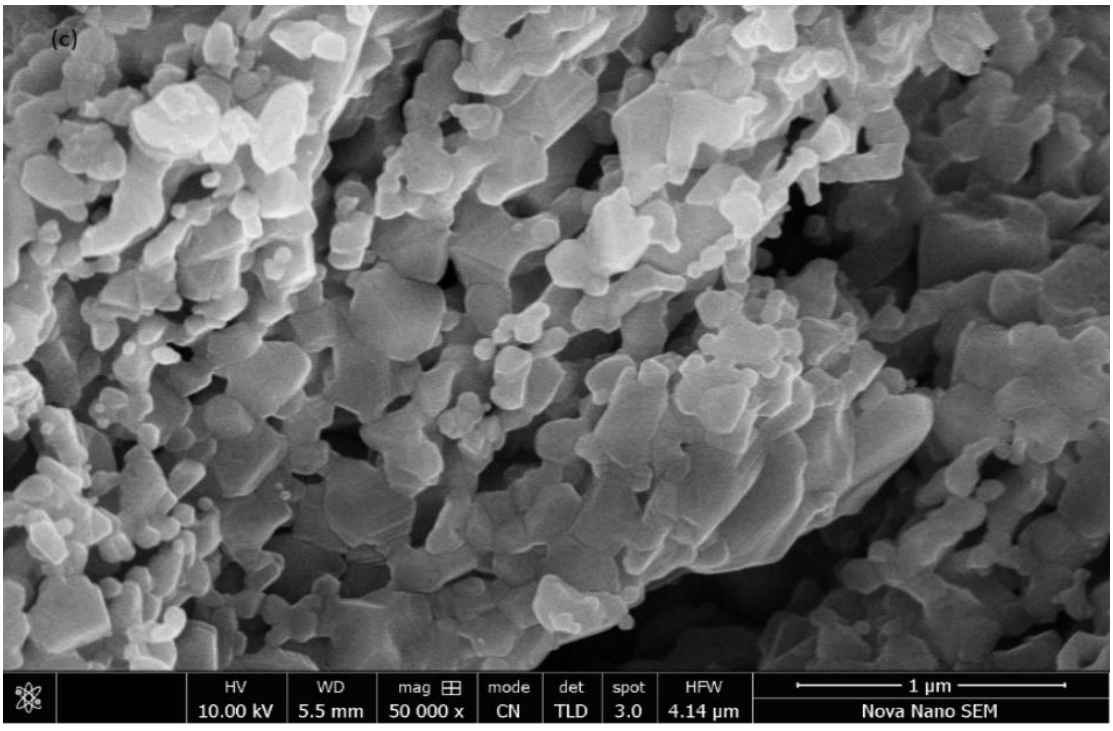

Figure 4.5: SEM Image of Nikel Oxide NiO / Potato Peels (20ml)

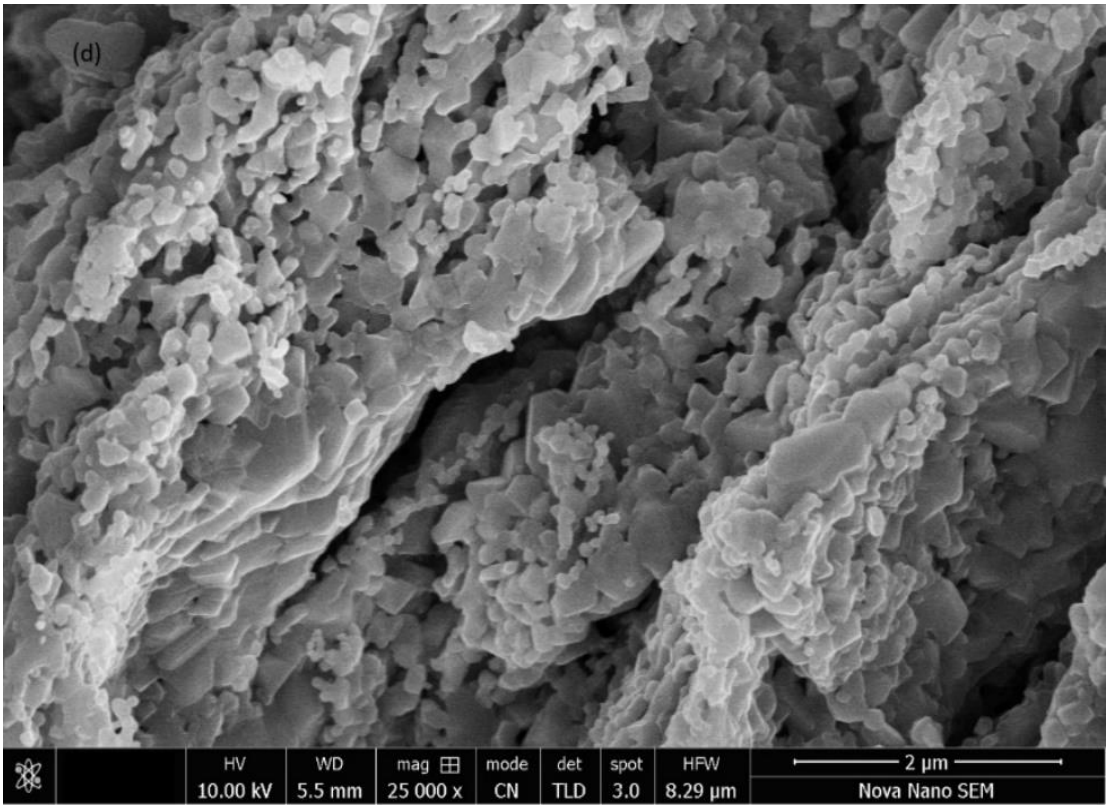

Figure 4.6: SEM Image of nickel Oxide NiO / Potato Peels (30ml)

Table 4.2. Sample grain Size

Sample No	Material	Size
1	NiO	201.0 nm
2	NiO/Potato Peels (10ml)	360.4 nm
3	NiO/Potato Peels (20ml)	219.6 nm
4	NiO/Potato Peels (30ml)	329.9 nm

Conclusion

NiO and NiO-containing potato peel extract (10ml, 20ml, and 30ml) were successfully synthesized as nanoparticles by hydrothermal treatment. A number of behavioral methods have been used to identify products. XRD confirmed the single-phase structure with lattice parameters raised from 8.38Å to 8.33Å. Agglomerated and heterogeneous nanoparticles were observed in SEM micrographs. After evaluating the ultra-fine nature and small crystallite size of NiO/Potato Peels nanocomposites, the fluoride adsorption tests will be carried out as a function of different pH of solution and with varying time. The Pseudo first and second order tests will be employed to confirm whether fluoride ions are absorbed onto the adsorbent (NiO/Potato Peels nanocomposite) physically or chemically. These adsorbents then will be used for treating the fluoride contaminated water of different areas of Punjab where fluoride contents are higher than the WHO limit.

CHAPTER 5

REFERENCES

References:

[1] Taniguchi, N. (1974). "On the basic concept of nanotechnology." Proceeding of the ICPE.

[2] Bhat, J. S. (2003). "Heralding a new future–Nanotechnology?" Current Science **85**(2): 147-154.

[3] Bohr, M. T. (2002). "Nanotechnology goals and challenges for electronic applications." IEEE Transactions on Nanotechnology **1**(1): 56-62.

[4] Thakkar, K. N., S. S. Mhatre and R. Y. Parikh (2010). "Biological synthesis of metallic nanoparticles." Nanomedicine: nanotechnology, biology and medicine **6**(2): 257-262.

[5] Madkour, L. H. (2018). "Biogenic–biosynthesis metallic nanoparticles (MNPs) for pharmacological, biomedical and environmental nanobiotechnological applications." Chron. Pharm. Sci. J **2**(1): 384-444.

[6] Madkour, L. H. (2018). "Biogenic–biosynthesis metallic nanoparticles (MNPs) for pharmacological, biomedical and environmental nanobiotechnological applications." Chron. Pharm. Sci. J **2**(1): 384-444.

[7] Ju-Nam, Y. and J. R. Lead (2008). "Manufactured nanoparticles: an overview of their chemistry, interactions and potential environmental implications." Science of the total environment **400**(1-3): 396-414.

[8] De, M., P. S. Ghosh and V. M. Rotello (2008). "Applications of nanoparticles in biology." Advanced Materials **20**(22): 4225-4241.

[9] Lu, A. H., E. e. L. Salabas and F. Schüth (2007). "Magnetic nanoparticles: synthesis, protection, functionalization, and application." Angewandte Chemie International Edition **46**(8): 1222-1244.

[10] Ghosh Chaudhuri, R. and S. Paria (2012). "Core/shell nanoparticles: classes, properties, synthesis mechanisms, characterization, and applications." Chemical reviews **112**(4): 2373-2433.

[11] Poulose, S., T. Panda, P. P. Nair and T. Theodore (2014). "Biosynthesis of silver nanoparticles." Journal of nanoscience and nanotechnology **14**(2): 2038-2049.

[12] Vijayakumar, M., K. Priya, F. Nancy, A. Noorlidah and A. Ahmed (2013). "Biosynthesis, characterisation and anti-bacterial effect of plant-mediated silver nanoparticles using Artemisia nilagirica." Industrial Crops and Products **41**: 235-240.

[13] Parsons, J., J. Peralta-Videa and J. Gardea-Torresdey (2007). "Use of plants in biotechnology: synthesis of metal nanoparticles by inactivated plant tissues, plant extracts, and living plants." Developments in environmental science **5**: 463-485.

[14] Antonyraj, C. A., J. Jeong, B. Kim, S. Shin, S. Kim, K.-Y. Lee and J. K. Cho (2013). "Selective oxidation of HMF to DFF using Ru/γ-alumina catalyst in moderate boiling solvents toward industrial production." Journal of Industrial and Engineering Chemistry **19**(3): 1056-1059.

[15] Neville, F., N. A. Pchelintsev, M. J. Broderick, T. Gibson and P. A. Millner (2009). "Novel one-pot synthesis and characterization of bioactive thiol-silicate nanoparticles for biocatalytic and biosensor applications." Nanotechnology **20**(5): 055612.

[16] Staniland, S. S. (2007). "Magnetosomes: bacterial biosynthesis of magnetic nanoparticles and potential biomedical applications." Nanotechnologies for the Life Sciences.

[17] Fu, H., X. Yang, X. Jiang and A. Yu (2013). "Bimetallic Ag–Au nanowires: synthesis, growth mechanism, and catalytic properties." Langmuir **29**(23): 7134-7142.

[18] Luo, X., A. Morrin, A. J. Killard and M. R. Smyth (2006). "Application of nanoparticles in electrochemical sensors and biosensors." Electroanalysis: An International Journal Devoted to Fundamental and Practical Aspects of Electroanalysis **18**(4): 319-326.

[19] Murthy, S. K. (2007). "Nanoparticles in modern medicine: state of the art and future challenges." International journal of nanomedicine **2**(2): 129.

[20] Janković, N. Z. and D. L. Plata (2019). "Engineered nanomaterials in the context of global element cycles." Environmental Science: Nano **6**(9): 2697-2711.

[21] Chandran, S. P., M. Chaudhary, R. Pasricha, A. Ahmad and M. Sastry (2006). "Synthesis of gold nanotriangles and silver nanoparticles using Aloevera plant extract." Biotechnology progress **22**(2): 577-583.

[22] Enz, U. (1982). "Magnetism and magnetic materials: Historical developments and present role in industry and technology." Handbook of Ferromagnetic Materials **3**: 1-36.

[23] Yousefi, L. and O. M. Ramahi (2007). New artificial magnetic materials based on fractal hilbert curves. 2007 International workshop on Antenna Technology: Small and Smart Antennas Metamaterials and Applications, IEEE.

[24] Francavilla, T. L., R. A. Hein and D. H. Liebenberg (2013). Magnetic susceptibility of superconductors and other spin systems, Springer Science & Business Media.

[25] Krishnan, K. M. (2016). Fundamentals and applications of magnetic materials, Oxford University Press.

[26] Ewing, J. A. (1883). "On the production of transient electric currents in iron and steel conductors by twisting them when magnetised, or by magnetising them when twisted." Proceedings of the Royal Society of London **36**(228-231): 117-135.

[27] Kluge, J. A., A. V. Soloviev, C. W. Dean, B. Nelson, W. E. Avera, G. Valdes and B. K. Haus (2018). Magnetic signature of surface waves measured in a laboratory experiment. OCEANS 2018 MTS/IEEE Charleston, IEEE.

[28] Finazzi, M., L. Duo and F. Ciccacci (2010). "Low-Dimensional Antiferromagnetic Oxides: An Overview." Magnetic Properties of Antiferromagnetic Oxide Materials: Surfaces, Interfaces, and Thin Films: 1-23.

[29] Hummel, R. E. (2011). Electrical properties of polymers, ceramics, dielectrics, and amorphous materials. Electronic properties of materials, Springer**:** 181-211.

[30] Carter, C. B. and M. G. Norton (2007). Ceramic materials: science and engineering, Springer.

[31] Batoo, K. M. and M. S. Ansari (2012). "Low temperature-fired Ni-Cu-Zn ferrite nanoparticles through auto-combustion method for multilayer chip inductor applications." Nanoscale research letters **7**(1): 1-14.

[32] Tolani, S. C., A. Golhar and K. Rewatkar (2019). A review of morphological, structural behaviour and technological applications of ferrites. AIP Conference Proceedings, AIP Publishing LLC.

[33] Pham, T. N., T. Q. Huy and A.-T. Le (2020). "Spinel ferrite (AFe 2 O 4)-based heterostructured designs for lithium-ion battery, environmental monitoring, and biomedical applications." RSC advances **10**(52): 31622-31661.

[34] Ganesh, I. (2013). "A review on magnesium aluminate (MgAl2O4) spinel: synthesis, processing and applications." International Materials Reviews **58**(2): 63-112.

[35] Moretti, R. and G. Ottonello (1998). "An appraisal of endmember energy and mixing properties of rare earth garnets." Geochimica et cosmochimica acta **62**(7): 1147-1173.

[36] Song, Z., D. Zhou and Q. Liu (2019). "Tolerance factor and phase stability of the garnet structure." Acta Crystallographica Section C: Structural Chemistry **75**(10): 1353-1358.

[37] Delacotte, C., G. Whitehead, M. Pitcher, C. Robertson, P. Sharp, M. Dyer, J. Alaria, J. Claridge, G. Darling and D. Allan (2018). "Structure determination and crystal chemistry of large repeat mixed-layer hexaferrites." IUCrJ **5**(6): 681-698.

[38] Stefan, I., R. Chiriac, V. Nicoara, N. Cioatera, C. Nicolicescu, M. Trotea and J. Ghercioiu (2011). PM Functional Materials: Research Regarding Structural Transformations of M Type Barium Ferrite Pirosynthesis. European Congress and Exhibition on Powder Metallurgy. European PM Conference Proceedings, The European Powder Metallurgy Association.

[39] Bamzai, K. and M. Bhat (2014). "Electrical and magnetic properties of some rare earth orthoferrites (RFeO3 where R= Y, Ho, Er) systems." Integrated Ferroelectrics **158**(1): 108-122.

[40] Assirey, E. A. R. (2019). "Perovskite synthesis, properties and their related biochemical and industrial application, Saudi Pharm." J **27**(6): 817-829.

[41] Geller, S. (1956). "Crystal structure of gadolinium orthoferrite, GdFeO3." The Journal of Chemical Physics **24**(6): 1236-1239.

[42] Sharma, U. S., R. N. Sharma and R. Shah (2014). "Physical and magnetic properties of manganese ferrite nanoparticles." International Journal of Engineering Research and Applications **4**(8): 14-17.

[43] Sharma, U., R. N. Sharma and R. Shah "Study of Physical and Magnetic properties of MnFe2O4 Nanoparticles."

[44] Manikandan, A., J. J. Vijaya, L. J. Kennedy and M. Bououdina (2013). "Structural, optical and magnetic properties of Zn1− xCuxFe2O4 nanoparticles prepared by microwave combustion method." Journal of molecular structure **1035**: 332-340.

[45] Manikandan, A., L. J. Kennedy, M. Bououdina and J. J. Vijaya (2014). "Synthesis, optical and magnetic properties of pure and Co-doped ZnFe2O4 nanoparticles by microwave combustion method." Journal of magnetism and magnetic materials **349**: 249-258.

[46] Phumying, S., S. Labuayai, E. Swatsitang, V. Amornkitbamrung and S. Maensiri (2013). "Nanocrystalline spinel ferrite (MFe2O4, M= Ni, Co, Mn, Mg, Zn) powders prepared by a simple aloe vera plant-extracted solution hydrothermal route." Materials Research Bulletin **48**(6): 2060-2065.

[47] AbuZeid, K. and L. Elhatow (2007). Impact of fluoride content in drinking water. Arab Water Healthy Conference Egypt: Cairo.

[48] Deng, J., Y. Liu, S. Liu, G. Zeng, X. Tan, B. Huang, X. Tang, S. Wang, Q. Hua and Z. Yan (2017). "Competitive adsorption of Pb (II), Cd (II) and Cu (II) onto chitosan-pyromellitic dianhydride modified biochar." Journal of colloid and interface science **506**: 355-364.

[49] Boldaji, M. R., A. Mahvi, S. Dobaradaran and S. Hosseini (2009). "Evaluating the effectiveness of a hybrid sorbent resin in removing fluoride from water." International Journal of Environmental Science & Technology **6**(4): 629-632.

[50] Kumar, S., A. Gupta and J. Yadav (2008). "Removal of fluoride by thermally activated carbon prepared from neem (Azadirachta indica) and kikar (Acacia arabica) leaves." Journal of Environmental Biology **29**(2): 227.

[51] Organization, W. H. (1984). Fluorine and fluorides, World Health Organization.

[52] Fu, F. and Q. Wang (2011). "Removal of heavy metal ions from wastewaters: a review." Journal of environmental management **92**(3): 407-418.

[53] Dąbrowski, A. (2001). "Adsorption—from theory to practice." Advances in colloid and interface science **93**(1-3): 135-224.

[54] Jamode, A., V. Sapkal and V. Jamode (2004). "Defluoridation of water using inexpensive adsorbents." Journal of the Indian Institute of Science **84**(5): 163.

[55] Karthikeyan, G. and S. S. Ilango (2007). "Fluoride sorption using Morringa Indica-based activated carbon." Journal of Environmental Health Science & Engineering **4**(1): 21-28.

[56] Ahmad, F., X. Liu, Y. Zhou, H. Yao, F. Zhao, Z. Ling and C. Xu (2016). "Assessment of thyroid endocrine system impairment and oxidative stress mediated by cobalt ferrite (CoFe2O4) nanoparticles in zebrafish larvae." Environmental toxicology **31**(12): 2068-2080.

[57] Predescu, A., E. Matei, A. Predescu, C. Predescu, C. Covaliu and R. Trusca (2015). Advanced materials with photocatalytic properties and magnetic core for environmental applications. Advanced Materials Research, Trans Tech Publ.

[58] Reddy, D. H. K. and Y.-S. Yun (2016). "Spinel ferrite magnetic adsorbents: alternative future materials for water purification?" Coordination Chemistry Reviews **315**: 90-111.

[59] Xiao, Y., H. Liang, W. Chen and Z. Wang (2013). "Synthesis and adsorption behavior of chitosan-coated MnFe2O4 nanoparticles for trace heavy metal ions removal." Applied Surface Science **285**: 498-504.

[60] Hashemian, S. (2010). "MnFe2O4/bentonite nano composite as a novel magnetic material for adsorption of acid red 138." African Journal of Biotechnology **9**(50): 8667-8671.

[61] Li, Y., S. Zhu, Q. Liu, Z. Chen, J. Gu, C. Zhu, T. Lu, D. Zhang and J. Ma (2013). "N-doped porous carbon with magnetic particles formed in situ for enhanced Cr (VI) removal." Water research **47**(12): 4188-4197.

[62] Andrade, R. G., D. Ferreira, S. R. Veloso, C. Santos-Pereira, E. M. Castanheira, M. Côrte-Real and L. R. Rodrigues (2022). "Synthesis and cytotoxicity assessment of citrate-coated calcium and manganese ferrite nanoparticles for magnetic hyperthermia." Pharmaceutics **14**(12): 2694.

[63] Kalaiselvan, C. R., S. S. Laha, S. B. Somvanshi, T. A. Tabish, N. D. Thorat and N. K. Sahu (2022). "Manganese ferrite (MnFe2O4) nanostructures for cancer theranostics." Coordination Chemistry Reviews **473**: 214809.

[64] Chaudhari, A., T. Kaida, H. B. Desai, S. Ghosh, R. P. Bhatt and A. R. Tanna (2022). "Dye degradation and antimicrobial applications of manganese ferrite nanoparticles synthesized by plant extracts." Chemical Physics Impact **5**: 100098.

[65] Amulya, M. S., H. Nagaswarupa, M. A. Kumar, C. Ravikumar and K. Kusuma (2021). "Sonochemical synthesis of MnFe2O4 nanoparticles and their electrochemical and photocatalytic properties." Journal of Physics and Chemistry of Solids **148**: 109661.

[66] Shakir, I., P. O. Agboola and S. Haider (2021). "Manganese spinel ferrite-reduced graphene oxides nanocomposites for enhanced solar irradiated catalytic studies." Ceramics International **47**(20): 28367-28376.

[67] Sivakumar, A., S. Sahaya Jude Dhas, P. Sivaprakash, A. I. Almansour, R. Suresh Kumar, N. Arumugam, K. Perumal, S. Arumugam and S. Martin Britto Dhas (2022). "Raman Spectroscopic and Electrochemical Measurements of Dynamic Shocked MnFe2O4 Nano-crystalline Materials." Journal of Inorganic and Organometallic Polymers and Materials **32**(1): 344-352.

[68] Sharifi, S., A. Yazdani and K. Rahimi (2020). "Incremental substitution of Ni with Mn in NiFe2O4 to largely enhance its supercapacitance properties." Scientific Reports **10**(1): 1-15.

[69] Sharma, U. S., R. N. Sharma and R. Shah (2014). "Physical and magnetic properties of manganese ferrite nanoparticles." International Journal of Engineering Research and Applications **4**(8): 14-17.

[70] Elkony, D. (2004). "Study of dielectric and impedance properties of Mn ferrites." Egypt J Sol **27**: 285-296.

[71] Rashad, M. (2006). "Synthesis and magnetic properties of manganese ferrite from low grade manganese ore." Materials Science and Engineering: B **127**(2-3): 123-129.

[72] Frolova, L., M. Kharytonov, I. Klimkina, O. Kovrov and A. Koveria (2020). Adsorption purification of waste water from chromium by ferrite manganese. E3S Web of Conferences, EDP Sciences.

[73] Zipare, K., J. Dhumal, S. Bandgar, V. Mathe and G. Shahane (2015). "Superparamagnetic manganese ferrite nanoparticles: synthesis and magnetic properties." Journal of Nanoscience and Nanoengineering **1**(3): 178-182.

[74] Khaleghi, M., H. Moradmard and S. F. Shayesteh (2017). "Cation distributions and magnetic properties of Cu-doped nanosized MnFe 2 O 4 synthesized by the coprecipitation method." IEEE Transactions on Magnetics **54**(1): 1-5.

[75] Singh, G. and S. Chandra (2019). "Copper Doped Manganese Ferrites PANI for Fabrication of Binder-Free Nanohybrid Symmetrical Supercapacitors." Journal of the Electrochemical Society **166**(6): A1154.

[76] Ata, S., I. Shaheen, F. Majid, I. Bibi, K. Jilani, Y. Slimani and M. Iqbal (2021). "Hydrothermal route for the synthesis of manganese ferrite nanoparticles and photocatalytic activity evaluation for the degradation of methylene blue dye." Zeitschrift für Physikalische Chemie **235**(11): 1433-1445.

[77] Sundriyal, S., V. Shrivastav, A. Kaur, A. Deep and S. R. Dhakate (2021). "Surface and diffusion charge contribution study of neem leaves derived porous carbon electrode for supercapacitor applications using acidic, basic, and neutral electrolytes." Journal of Energy Storage **41**: 103000.

[78] Nzekekwu, A. and O. Abosede (2019). "Green synthesis and characterization of silver nanoparticles using leaves extracts of neem (Azadirachta indica) and bitter leaf (Vernonia amygdalina)." Journal of Applied Sciences and Environmental Management **23**(4): 695-699.

[79] Kumari, R., A. Dwivedi, R. Kumar, M. K. Gundawar and A. K. Rai (2022). "Optical characterization of Azadirachta Indica (Neem) leaves using spectroscopic techniques." Journal of Optics: 1-16

[80] Byrappa, K. and M. Haber (2001). Hydrothermal technology for crystal growth, Noyes Publications [Imprint].

[81] Elliott, D. C. (2011). Hydrothermal processing, Pacific Northwest National Lab.(PNNL), Richland, WA (United States).

[82] Seyfried, W., D. R. Janecky, M. E. Berndt, G. Ulmer and H. Barnes (1987). "Rocking autoclaves for hydrothermal experiments II. The flexible reaction-cell system." Hydrothermal experimental techniques **23**.

[83] Liu, N., X. Chen, J. Zhang and J. W. Schwank (2014). "A review on TiO2-based nanotubes synthesized via hydrothermal method: Formation mechanism, structure modification, and photocatalytic applications." Catalysis Today **225**: 34-51.

[84] Macklen, E. (1968). "Influence of atmosphere on the thermal decomposition of some transition metal oxalates." Journal of Inorganic and Nuclear Chemistry **30**(10): 2689-2695.

[85] Mostafa, N. Y., M. Hessien and A. A. Shaltout (2012). "Hydrothermal synthesis and characterizations of Ti substituted Mn-ferrites." Journal of alloys and compounds **529**: 29-33.

[86] Mostafa, N., E. Kishar and S. Abo-El-Enein (2009). "FTIR study and cation exchange capacity of Fe3+-and Mg2+-substituted calcium silicate hydrates." Journal of alloys and compounds **473**(1-2): 538-542.

[87] Gan, Y. X., A. H. Jayatissa, Z. Yu, X. Chen and M. Li (2020). Hydrothermal synthesis of nanomaterials, Hindawi. **2020**.

[88] Qin, A.-M., Y.-P. Fang, H.-D. Ou, H.-Q. Liu and C.-Y. Su (2005). "Formation of various morphologies of covellite copper sulfide submicron crystals by a hydrothermal method without surfactant." Crystal growth & design **5**(3): 855-860.

[89] Polini, A. and F. Yang (2017). Physicochemical characterization of nanofiber composites. Nanofiber composites for biomedical applications, Elsevier**:** 97-115.

[90] Lauridsen, E., S. Schmidt, S. F. Nielsen, L. Margulies, H. Poulsen and D. J. Jensen (2006). "Non-destructive characterization of recrystallization kinetics using three-dimensional X-ray diffraction microscopy." Scripta materialia **55**(1): 51-56.

[91] Bunaciu, A. A., E. G. UdriŞTioiu and H. Y. Aboul-Enein (2015). "X-ray diffraction: instrumentation and applications." Critical reviews in analytical chemistry **45**(4): 289-299.

[92] Warren, B. E. (1990). X-ray Diffraction, Courier Corporation.

[93] Lee, M. (2019). "X-ray diffraction for materials research."

[94] Chauhan, A. and P. Chauhan (2014). "Powder XRD technique and its applications in science and technology." J Anal Bioanal Tech **5**(5): 1-5.

[95] Terinte, N., R. Ibbett and K. C. Schuster (2011). "Overview on native cellulose and microcrystalline cellulose I structure studied by X-ray diffraction (WAXD): Comparison between measurement techniques." Lenzinger Berichte **89**(1): 118-131.